











Identification of 1,2,3-triazole-phthalimide derivatives as potential drugs against COVID-19: a virtual screening, docking and molecular dynamic study

Vanderlan Nogueira Holanda^{a,b} , Elton Marlon de Araújo Lima^{b,c} , Welson Vicente da Silva^b ,
Rafael Trindade Maia^d , Rafael de Lima Medeiros^e , Arabinda Ghosh^f , Vera Lúcia de Menezes Lima^{a*} 
and Regina Celia Bressan Queiroz de Figueiredo^{b*} 

^aLaboratório de Lipídios e Aplicação de Biomoléculas em Doenças Prevalentes e Negligenciadas, Departamento de Bioquímica, Centro de Biociências, Universidade Federal de Pernambuco, Recife, Pernambuco, Brazil; ^bLaboratório de Biologia Celular de Patógenos, Instituto Aggeu Magalhães, Departamento de Microbiologia, Instituto Aggeu Magalhães – IAM/FIOCRUZ-PE, Recife, Pernambuco, Brazil; ^cLaboratório de Polímeros Não-Convencionais, Departamento de Física, Centro de Ciências Exatas e da Natureza, Universidade Federal de Pernambuco, Recife, Pernambuco, Brazil; ^dCentro de Desenvolvimento Sustentável do Semiárido, Universidade Federal de Campina Grande, Sumé, Paraíba, Brazil; ^eInstituto de Física, Universidade Federal de Alagoas, Maceió, Alagoas, Brazil; ^fMicrobiology Division, Department of Botany, Gauhati University, Guwahati, Assam, India

Communicated by Ramaswamy H. Sarma

ABSTRACT

In this work we aimed to perform an *in silico* predictive screening, docking and molecular dynamic study to identify 1,2,3-triazole-phthalimide derivatives as drug candidates against SARS-CoV-2. The *in silico* prediction of pharmacokinetic and toxicological properties of hundred one 1,2,3-triazole-phthalimide derivatives, obtained from SciFinder® library, were investigated. Compounds that did not show good gastrointestinal absorption, violated the Lipinski's rules, proved to be positive for the AMES test, and showed to be hepatotoxic or immunotoxic in our ADMET analysis, were filtered out of our study. The hit compounds were further subjected to molecular docking on SARS-CoV-2 target proteins. The ADMET analysis revealed that 43 derivatives violated the Lipinski's rules and 51 other compounds showed to be positive for the toxicity test. Seven 1,2,3-triazole-phthalimide derivatives (**A7**, **A8**, **B05**, **E35**, **E38**, **E39**, and **E40**) were selected for molecular docking and MFCC—*ab initio* analysis. The results of molecular docking pointed the derivative **E40** as a promising compound interacting with multiple target proteins of SARS-CoV-2. The complex **E40-M^{Pro}** was found to have minimum binding energy of -10.26 kcal/mol and a general energy balance, calculated by the quantum mechanical analysis, of -8.63 eV. MD simulation and MMGBSA calculations confirmed that the derivatives **E38** and **E40** have high binding energies of -63.47 ± 3 and -63.31 ± 7 kcal/mol against SARS-CoV-2 main protease. In addition, the derivative **E40** exhibited excellent interaction values and inhibitory potential against SARS-CoV-2 main protease and viral nucleocapsid proteins, suggesting this derivative as a potent antiviral for the treatment and/or prophylaxis of COVID-19.

Abbreviations: **3CLPro:** 3-C Like Protease; **ACE2:** Angiotensin Converting Enzyme 2; **ADME:** Absorption, Distribution, Metabolism and Excretion; **ALA:** Alanine; **ARDS:** Acute Respiratory Discomfort Syndrome; **ARG:** Arginine; **BBB:** Blood-Brain Barrier; **ClogP:** Octanol-water partition coefficient; **Comp:** Compounds; **COVID-19:** Coronavirus Disease 2019; **CYS:** Cysteine; **DNA:** Deoxyribonucleic Acid; **E:** Total Energy; **Elec:** Electrostatic; **GIA:** Gastrointestinal Absorption; **GLN:** Glutamine; **GLU:** Glutamic Acid; **GLY:** Glycine; **HB:** Hydrogen-bond; **HBA:** Hydrogen-Bond Acceptors; **HBD:** Hydrogen-Bond Donors; **HEP:** Hepatotoxicity; **HERG:** Human Ether-a-go-go-related Gene; **HIS:** Histidine; **HIV:** Human Immunodeficiency Virus; **ILE:** Isoleucine; **IT:** Immunotoxicity; **K_i:** Inhibition Constant; **LYS:** Lysine; **MET:** Methionine; **MFCC:** Molecular Fractionation with Conjugate Caps; **M^{Pro}:** Main Protein; **MTD:** Maximum Tolerated Dose; **MW:** Molecular Weight; **NCP:** Nucleocapsid Protein; **NRB:** Number Rotatable Bonds; **NSP:** Non-structural Proteins; **ORAT:** Acute Oral Toxicity in Rats; **ORCT:** Oral Rat Chronic Toxicity; **PDB:** Protein Data Bank; **PGs:** P-glycoprotein Substrate; **PHE:** Phenylalanine; **PSA:** Polar Surface Area; **RBD:** Receptor Binding Domain; **RNA:** Ribonucleic Acid; **RO5:** Lipinski's Rule of Five; **SARS-CoV-2:** Severe acute respiratory syndrome coronavirus 2; **SS:** Skin Sensitization; **TC:** Total Clearance; **TRP:** Tryptophan; **TYR:** Tyrosine; **VAL:** Valine; **VDW:** van der Waals; **MD:** Molecular Dynamic; **MMGBSA:** Molecular mechanics and generalized Born and surface area

ARTICLE HISTORY


Received 8 September 2020
Accepted 28 December 2020

KEYWORDS

Antiviral; SARS-CoV-2;
phthalimide; 123-triazole;
MD simulation

CONTACT Vanderlan Nogueira Holanda  vanderlan.holanda@ufpe.br  Laboratório de Lipídios e Aplicação de Biomoléculas em Doenças Prevalentes e Negligenciadas, Departamento de Bioquímica, Centro de Biociências, Universidade Federal de Pernambuco, Recife, Pernambuco, Brazil;  Laboratório de Biologia Celular de Patógenos, Instituto Aggeu Magalhães, Departamento de Microbiologia, Instituto Aggeu Magalhães – IAM/FIOCRUZ-PE, Avenida Professor Moraes Rego s/n 50670-420, Recife, Pernambuco, Brazil.

*Both authors contributed equally to this work.

 Supplemental data for this article can be accessed online at <https://doi.org/10.1080/07391102.2020.1871073>.

1. Introduction

Nowadays respiratory diseases caused by virus are among the main causes of morbidity and mortality due to their easy spreading and the high pathogenicity of viral agents (Piñana et al., 2020). At the end of 2019 a new Coronavirus, called SARS-CoV-2, appeared in Wuhan, China and became one of the most aggressive pandemics in history (Meo et al., 2020), exceeding 3 million infected individuals and causing thousands of deaths worldwide by the beginning of May 2020. The clinical manifestations of Coronavirus disease 2019 (COVID-19) are characterized by fever, fatigue, cough, which can rapidly progress into Acute Respiratory Discomfort Syndrome (ARDS) and death (Huang et al., 2020). Although vaccinal candidates against COVID-19 are already under development stage, a safe and effective vaccine for large-scale vaccination is far from becoming a reality. Hydroxychloroquine or chloroquine alone or in combination with a second-generation of macrolide, have been preconized for the treatment of COVID-19 despite no conclusive evidence of their benefits (Mehra et al., 2020). In this regard, the search for a safe and effective treatment against the severe form of COVID-19 is still necessary (Zhang et al., 2020).

Among the arsenal of bioactive compounds, the 1,2,3-triazole group has been attracting interest of scientific community due to their wide-ranging and versatile medicinal applications such as antivirals (Sun et al., 2020), antibacterial (Gonzaga et al., 2013), antifungal (Thanh et al., 2019) and antiparasitic (Leite et al., 2018) agents. Furthermore, 1,2,3-triazoles can be easily synthesized by low-cost copper catalysed reactions between alkynes and azides, namely *click chemistry*. Besides being used to synthesize triazoles derivatives, *click chemistry* is also widely applied for the fusion of two or more chemical groups in a single hybrid molecule with improved biological activity (Ouyang et al., 2018). As triazole derivatives, the phthalimide group has been shown to be useful in the formation of hybrid compounds with antiviral activity against HIV (Al-Masoudi et al., 2016), cytomegalovirus and varicella-zoster (Mandić et al., 2020). Importantly, both triazole and phthalimide derivatives also have relevant anti-inflammatory activity (Assis et al., 2019). Therefore, 1,2,3-triazole-phthalimide hybrids may not only be able to prevent viral replication but also treat the severe form of COVID-19, characterized by an intense inflammatory process called “cytokine storm” (Zhang et al., 2020).

One of the strategies for the discovery of antiviral candidates against SARS-CoV-2 is the association of *in silico* screening-based approaches with the molecular docking of selected molecules against SARS-CoV-2 target proteins, to identify compounds having good drug-likeness properties. Because experimental approaches for drug discovery are highly costly and time-consuming, screening-based methods offer a fast and low-cost way for prospecting new potential drugs (Hall & Ji, 2020). The SARS-CoV-2 viral genome encodes for 29 proteins—many of which could serve as potential targets for anti-viral drugs. Among these proteins, spike protein (S), C-like proteases and nucleocapsid proteins have gained growing interest due to their relevant roles in the host cell recognition, viral replication, processing and formation of nucleocapsid structure. Spike glycoproteins, found on the surface of SARS-CoV-2, are a class I fusion proteins which bind to human Angiotensin Converting

Enzyme 2 (ACE2) receptor mediating both the fusion of the viral envelope with the host-cell membrane and the virus entry into host cells. The chymotrypsin-like cysteine protease, also known as main protease (M^{Pro}) or 3-C like protease (3CLPro), is also an interesting target for drugs against COVID-19. This protease cleaves the C-terminal sequence of the polyprotein PP1A and PP1AB into 16 functional non-structural proteins (nsps), which play an important role in viral replication (Chen et al., 2020). Besides proteases and spike proteins, the nucleocapsid protein of SARS-CoV-2 has been investigated as a target protein for drug development. The nucleocapsid protein comprises two structured domains, the N-terminal domain (NTD) and the C-terminal domain (CTD), interspersed by three intrinsically disordered regions (IDRs) known as the N-terminal arm (N-arm), the central linker region (LKR), and the C-terminal tail (C-tail) arm (Zhou et al., 2008, 2020). The main function of these proteins is to form complexes with ribonucleoproteins. However, they also regulate the replication, transcription of viral RNA and, in the host cells, inhibit protein translation, leading to disruption of host cell metabolism. Hence, targeting this protein can lead to blockbuster therapeutic agents for COVID-19 treatment (Bhatia, Narang & Rawal, 2020; Zeng et al., 2008). In this study, we have performed docking study of selected 1,2,3-triazole-phthalimide derivatives against COVID-19 targets.

2. Materials and methods

2.1. Selection and preparation of ligands

The access to the chemical structures of 1,2,3-triazole-phthalimide hybrid compounds was performed using the SciFinder® database (<https://scifinder.cas.org>). For this study, only compounds that were obtained by *click chemistry* and have biological activity already reported in the literature were chosen for the analysis. The chemical structure of compounds was built using ACD/ChemSketch 2.1 and optimized using the PM3 semi-empirical method (Stewart, 1989) implemented in Mercury 4.3.1 (Macrae et al., 2008). The protonation states of the ligands were verified by MarvinSketch 20.19.0 software assuming a physiological pH (Butcher et al., 2015). The canonical smiles were obtained for ADMET *in silico* analysis (Karwath & Raedt, 2006).

2.2. *In silico* analysis of physico-chemical, pharmacokinetic and toxicological profile (ADMET) of ligands

The analysis of the pharmacokinetic and druglike properties of 1,2,3-triazole-phthalimide derivatives was carried out using the Web server SwissADME, <http://www.swissadme.ch/> (Swiss Institute of Bioinformatics). Only the compounds that have good gastrointestinal adsorption and did not violate the following parameters of Lipinski's Rule of Five: (i) $\text{clogP} \leq 5$; (ii) Molecular weight (MW) ≤ 500 g/mol; (iii) Number of hydrogen bond acceptors (HBA) (sum of N and O atoms) ≤ 10 , (iv) Number of hydrogen bond donors (HBD) (sum of OH and NH groups) ≤ 5 , were selected (Lipinski, 2004). The number of rotatable bonds (n_{Rotb}) ≤ 10 , were also considered for the further toxicity and molecular docking analysis. The prediction of

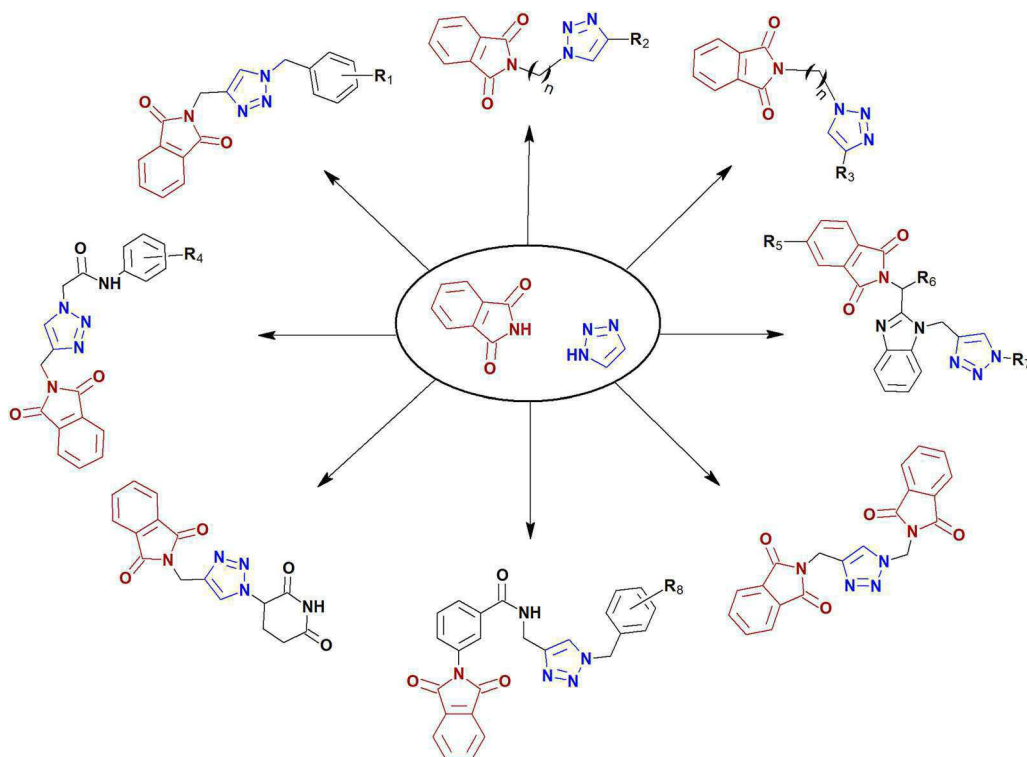


Figure 1. The chemical structures of 1,2,3-triazole-phthalimide bioactive derivatives obtained from SciFinder database. R₁: 4-methylbenzyl 2-methylbenzyl, 4-methoxybenzyl, 2-fluorobenzyl, 3-fluorobenzyl, 4-fluorobenzyl, 2-chlorobenzyl, 3-chlorobenzyl, 2,3-dichlorobenzyl, 3,4-dichlorobenzyl, 2-bromobenzyl, 4-bromobenzyl, 2-nitrobenzyl; R₂: 2-(methylsulfanyl)-1,3-benzothiazole or phenyl; R₃: carbohydrate or phthalimide; R₄: 4-methyl, 4-chloro, H, 4-bromo, 3-nitro, 4-methoxy, 2-chloro, 3-chloro, 4-fluoro, 2-methoxy, 2-methyl; R₅: Methyl or H; R₆: methylbutyl, methyl and 2-methylpropyl; R₇: 4-fluorophenyl, p-tolyl, H, 1-pentafluorophenyl, 4-(trifluoromethyl)phenyl, 1-benzyl, 1-phenyl, 4-methoxyphenyl, 2,4-difluorophenyl, 2,6-difluorophenyl, 1-perfluorophenyl, 2-fluorophenyl, 4-pyridinyl; R₈: H, 4-methoxybenzyl, 2-fluorobenzyl, 4-fluorobenzyl, 4-chlorobenzyl, 2,6-dichlorobenzyl, 3-bromobenzyl, 4-bromobenzyl, 2-nitrobenzyl, 3-nitrobenzyl, 4-nitrobenzyl.

toxicological potential of these compounds was performed using the pKCSM on-line platforms (Pires et al., 2015). The AMES toxicity, hepatotoxicity, and immunotoxicity parameters were also used to filter out compounds.

2.3. Molecular docking of 1,2,3-triazole-phthalimide hybrids on SARS-CoV-2 target proteins

The molecular docking of selected compounds on SARS-CoV-2 target proteins was carried out using iGemDock 2.1 and AutoDock 4.2 software. The main protease (M^{Pro}), spike (SP) and viral nucleocapsid (NCP) proteins were chosen according to the stereochemical parameters provided by Ramachandran analysis, using the PROCHECK server (Laskowski et al., 2006). Molecular docking was performed based on the confrontation between optimized ligands structure and biomacromolecules from SARS-CoV-2. The crystal structure of viral proteins was obtained from the Protein Data Bank (PDB) under the codes: spike: 6VSB, in its open (6VYB) and closed states (6VXX) (Walls et al., 2020; Wrapp et al., 2020); nucleocapsid protein, 6VYO (Yadav et al., 2020) and M^{Pro}, 5R80 (Razzaghi-Asl et al., 2020). The validation of target protein-ligand complex structures was performed using the co-crystallized standard ligand of target proteins to ensure the virtual screening process. For this, M^{Pro} was redocked with its co-crystallized ligand RGZ: methyl 4-sulfamoylbenzoate. For each ligand-protein complex 10-docking poses were generated using Lamarckian Genetic Algorithm (López-Camacho et al., 2015). The pose with the lowest

binding energy was selected as the final docking result. The interactions of the target-ligand complex were analysed and rendered using Discovery Studio v.20.1.0.19295.

2.4. Molecular fractionation with conjugate caps (MFCC—ab initio)

To calculate the interaction energy between receptors and ligands, the complexes obtained by molecular docking were used as an input for the molecular fractionation method with conjugated caps (MFCC). For this purpose, a convergence radius of 15 Å was defined (having its origin in the geometric center of the ligands). All the residues with at least one atom inside the spherical volume were taken into account. All atomic positions were kept fixed, with the exception of hydrogen atoms, which were optimized using consistent valence force field (CVFF). Subsequently, simulations within the Density Functional Theory formalism using the Local Density Approximation (DFT/LDA) were carried out using the DMOL3 code.

To obtain the interaction energy between each eligible amino acid and the ligands, a fractionation was applied, respecting Eq. (1):

$$E(L - R^i) = E(L - C^{(i-1)}R^iC^{(i+1)}) - E(C^{(i-1)}R^iC^{(i+1)}) \\ - E(L - C^{(i-1)}C^{(i+1)}) + E(C^{(i-1)}C^{(i+1)})$$

where $E(L - R^i)$ represents the interaction energy between the ligand L and the amino acid R^i , where cap $C^{(i-1)}$ and $C^{(i+1)}$ is arranged including the predecessor amino acid and posteriorly

Table 1. Analysis of physicochemical and pharmacokinetic profiles of selected phthalimide-1,2,3-triazole derivatives.

	Physicochemical properties					Absorption		Metabolism					Excretion TC
	HBA	HBD	CLogP	MW	NRB	BBB	PGP	1A2	2C19	2C9	2D6	3A4	
A01	4	0	2.47	332.36	4	Yes	No	Yes	Yes	Yes	No	No	-0.07
A02	4	0	2.43	332.36	4	Yes	No	Yes	Yes	Yes	No	No	-0.06
A03	5	0	2.10	348.36	5	No	No	Yes	Yes	Yes	No	Yes	-0.04
A04	5	0	2.42	336.32	4	Yes	No	Yes	Yes	Yes	No	No	0.15
A05	5	0	2.42	336.32	4	Yes	No	Yes	Yes	Yes	No	No	0.12
A06	5	0	2.44	336.32	4	Yes	No	Yes	Yes	Yes	No	No	0.10
A07	4	0	2.63	352.77	4	Yes	No	Yes	Yes	Yes	No	No	0.34
A08	4	0	2.64	352.77	4	Yes	No	Yes	Yes	Yes	No	No	0.28
A09	4	0	3.15	387.22	4	Yes	No	Yes	Yes	Yes	No	No	0.46
A10	4	0	3.17	387.22	4	Yes	No	Yes	Yes	Yes	No	No	0.40
A11	4	0	2.71	397.23	4	Yes	No	Yes	Yes	Yes	No	No	0.32
A12	4	0	2.75	397.23	4	Yes	No	Yes	Yes	Yes	No	No	0.25
A13	6	0	1.49	363.33	5	No	No	No	Yes	No	No	No	-0.07
B01	5	0	3.03	407.47	5	No	No	Yes	Yes	Yes	No	Yes	0.41
B02	5	0	3.19	421.50	6	No	No	Yes	Yes	Yes	No	Yes	0.49
B05	4	0	2.04	304.30	3	Yes	No	Yes	Yes	No	No	No	0.11
B06	4	0	2.23	318.33	4	Yes	No	Yes	Yes	Yes	No	No	0.11
B07	4	0	2.54	332.36	5	Yes	No	Yes	Yes	Yes	No	No	0.19
B08	4	0	2.87	346.38	6	Yes	No	Yes	Yes	Yes	No	Yes	0.15
C01	10	0	1.03	484.46	11	No	No	No	No	No	No	Yes	1.37
C04	6	0	1.46	401.37	5	No	Yes	No	Yes	Yes	No	Yes	-0.23
C05	6	0	1.78	415.40	6	No	Yes	No	Yes	Yes	No	Yes	-0.14
C06	6	0	2.09	429.43	7	No	Yes	No	Yes	Yes	No	Yes	-0.13
D01	5	1	1.75	375.38	6	No	Yes	No	No	Yes	No	Yes	-0.07
D02	5	1	1.92	395.80	6	No	No	No	Yes	Yes	No	Yes	0.05
D03	5	1	1.41	361.35	6	No	Yes	No	No	No	No	No	-0.07
D04	5	1	2.06	440.25	6	No	No	No	Yes	Yes	No	Yes	0.03
D06	6	1	1.45	391.38	7	No	Yes	No	No	Yes	No	Yes	-0.05
D07	5	1	2.00	395.80	6	No	No	No	Yes	Yes	No	Yes	0.32
D08	5	1	1.94	395.80	6	No	No	No	Yes	Yes	No	Yes	0.11
D09	6	1	1.72	379.34	6	No	No	No	No	No	No	No	-0.24
D10	6	1	1.46	391.38	7	No	Yes	No	No	Yes	No	Yes	-0.11
D11	6	1	1.42	391.38	7	No	Yes	No	No	Yes	No	Yes	0.02
D12	5	1	1.75	375.38	6	No	Yes	No	No	Yes	No	Yes	-0.06
E03	5	1	3.37	430.50	6	No	No	No	Yes	Yes	Yes	Yes	0.51
E21	6	0	3.31	491.54	7	No	Yes	No	Yes	Yes	No	Yes	0.73
E25	6	0	3.47	466.47	5	No	Yes	No	Yes	Yes	No	No	0.54
E26	5	0	3.53	462.50	5	No	Yes	No	Yes	Yes	No	No	0.72
E27	5	0	3.22	448.48	5	No	Yes	No	Yes	Yes	No	No	0.71
E29	6	0	3.58	466.47	5	No	Yes	No	Yes	Yes	No	No	0.56
E31	5	0	3.29	462.50	5	No	Yes	No	Yes	Yes	No	Yes	0.81
E33	5	1	2.17	374.40	4	No	No	No	Yes	Yes	No	Yes	0.84
E35	5	0	3.90	476.53	5	No	Yes	No	Yes	Yes	No	Yes	0.72
E37	5	1	2.54	388.42	4	No	No	No	Yes	Yes	No	Yes	0.85
E38	5	0	3.62	462.50	5	No	Yes	No	Yes	Yes	No	No	0.72
E39	5	0	3.68	476.53	6	No	Yes	No	Yes	Yes	No	Yes	0.81
E40	6	0	2.89	463.49	5	No	Yes	No	Yes	Yes	No	Yes	0.76
E45	6	0	3.99	494.52	6	No	Yes	No	Yes	Yes	No	No	0.44
F01	6	1	0.33	325.28	2	No	No	No	No	No	No	No	-0.17
F02	6	1	0.24	339.31	3	No	No	No	No	No	No	No	-0.19
G01	5	1	2.87	437.45	7	No	Yes	No	Yes	Yes	No	Yes	0.05
G02	6	1	2.90	467.48	8	No	Yes	No	Yes	Yes	Yes	Yes	0.04
G03	6	1	3.19	455.44	7	No	Yes	No	Yes	Yes	No	Yes	-0.15
G04	6	1	3.21	455.44	7	No	Yes	No	Yes	Yes	No	Yes	-0.20
G05	5	1	3.36	471.90	7	No	Yes	No	Yes	Yes	No	Yes	-0.20
H01	6	0	1.39	387.35	4	No	Yes	No	Yes	No	No	No	-0.25
H02	6	0	1.33	387.35	4	No	Yes	No	Yes	No	No	No	-0.26

HBA: Hydrogen-Bond Acceptors, HBD: Hydrogen-Bond Donors, CLogP: Octanol-water partition coefficient, MW: Molecular Weight, NRB: Number Rotatable Bonds, BBB: Blood-Brain Barrier, PGP: P-glycoprotein Substrate, TC: Total Clearance (Log mL/min/kg).

respectively of R^i . The term $E(L - C^{(i-1)}R^iC^{(i+1)})$ is the total energy of the system consisting of the ligand and the residue with its caps; the $E(C^{(i-1)}R^iC^{(i+1)})$ is the total energy of the waste and the isolated caps $E(L - C^{(i-1)}R^iC^{(i+1)})$ the total energy of the system formed by the ligand and only the caps; and finally, $E(C^{(i-1)}C^{(i+1)})$ the energy of the system composed by the caps. The total energy of the ligand interaction with the entire receptor is obtained by adding the individual energy of each eligible amino acid, as in Eq. (2).

$$\sum_{i=1}^N E(L - R^i)$$

where N is the number of eligible amino acids.

2.5. Molecular dynamics and binding energy calculations

Molecular dynamics and simulation (MDS) studies were carried out in order to determine the stability and convergence

Table 2. *In silico* toxicological prediction of 1,2,3-triazole-phthalimide derivatives that showed better pharmacokinetic profile.

Comp.	AMES		ORAT						
	toxicity	MTD	hERGI	hERG II	(LD ₅₀)	ORCT	Hep	IT	SS
A01	No	-0.43	No	Yes	1.984	1.317	Yes	No	No
A02	No	-0.40	No	Yes	1.994	1.306	Yes	No	No
A03	Yes	-0.30	No	Yes	2.112	1.373	Yes	No	No
A04	No	-0.13	No	Yes	1.991	1.823	Yes	No	No
A05	Yes	-0.22	No	Yes	2.062	1.404	Yes	No	No
A06	No	-0.31	No	Yes	2.050	1.384	Yes	No	No
A07	No	-0.39	No	Yes	2.044	1.236	No	No	No
A08	No	-0.40	No	Yes	2.035	1.269	No	No	No
A09	No	-0.40	No	Yes	2.178	1.225	Yes	No	Yes
A10	No	-0.40	No	Yes	2.156	1.257	Yes	No	No
A11	No	-0.39	No	Yes	2.053	1.226	Yes	No	No
A12	No	-0.42	No	Yes	2.040	1.236	Yes	No	No
A13	Yes	-0.38	No	Yes	2.980	1.595	Yes	Yes	No
B01	No	0.38	No	Yes	2.309	0.850	Yes	No	No
B02	No	0.40	No	Yes	2.244	0.924	Yes	No	No
B05	No	0.48	No	Yes	2.541	1.133	No	No	No
B06	No	0.47	No	Yes	2.429	1.298	Yes	No	No
B07	No	0.51	No	Yes	2.460	1.411	Yes	No	No
B08	No	0.55	No	Yes	1.888	1.171	Yes	No	No
C01	No	0.63	No	No	2.439	1.309	Yes	No	No
C04	No	-0.14	No	Yes	2.272	2.020	Yes	No	No
C05	No	-0.13	No	Yes	2.243	2.046	Yes	No	No
C06	No	-0.09	No	Yes	2.221	1.992	Yes	No	No
D01	No	-0.21	No	Yes	2.153	1.674	Yes	No	No
D02	No	-0.18	No	Yes	2.148	1.631	Yes	No	No
D03	No	-0.25	No	Yes	2.109	1.696	Yes	No	No
D04	No	-0.19	No	Yes	2.158	1.624	Yes	No	No
D06	No	-0.14	No	Yes	2.080	1.654	Yes	No	No
D07	No	-0.25	No	Yes	2.151	1.625	Yes	No	No
D08	No	-0.22	No	Yes	2.171	1.693	Yes	No	No
D09	No	-0.12	No	Yes	2.065	1.605	Yes	No	No
D10	No	-0.25	No	Yes	2.093	1.648	Yes	No	No
D11	No	-0.21	No	Yes	2.111	1.691	Yes	No	No
D12	No	-0.28	No	Yes	2.155	1.668	Yes	No	No
E03	No	0.24	No	Yes	2.253	2.644	Yes	No	No
E21	No	0.23	No	Yes	2.480	1.690	Yes	No	No
E25	No	0.12	No	Yes	2.413	0.673	Yes	No	No
E26	Yes	0.08	No	Yes	2.416	0.803	No	No	No
E27	Yes	0.117	No	Yes	2.417	0.721	No	No	No
E29	Yes	0.121	No	Yes	2.416	0.555	Yes	No	No
E31	Yes	-0.028	No	Yes	2.435	0.822	No	No	No
E33	Yes	0.042	No	Yes	2.191	1.663	No	No	No
E35	No	0.200	No	Yes	2.463	1.074	No	No	No
E37	Yes	0.095	No	Yes	2.115	1.868	No	No	No
E38	No	0.217	No	Yes	2.465	0.993	No	No	No
E39	No	0.108	No	Yes	2.459	1.115	No	No	No
E40	No	0.225	No	Yes	2.441	1.590	No	No	No
E45	No	0.276	No	Yes	2.484	0.917	Yes	No	No
F01	No	-0.151	No	No	2.482	1.831	Yes	No	No
F02	No	0.095	No	No	2.364	1.965	Yes	No	No
G01	Yes	0.277	No	Yes	2.647	0.584	Yes	No	No
G02	Yes	0.236	No	Yes	2.853	0.578	Yes	No	No
G03	Yes	0.378	No	Yes	2.776	0.506	Yes	No	No
G04	Yes	0.292	No	Yes	2.816	0.532	Yes	No	No
G05	Yes	0.166	No	Yes	2.710	0.395	Yes	No	No
H01	No	0.015	No	Yes	2.110	1.889	Yes	No	No
H02	No	-0.018	No	Yes	2.216	1.985	Yes	No	No

MTD: Maximum Tolerated Dose—log(mg/kg/day), hERH I/II: Human Ether-a-go-go-related Gene, ORAT: Acute Oral Toxicity in Rats (LD₅₀)—mol/kg, ORCT: oral rat chronic toxicity log(mg/kg/day), Hep: Hepatotoxicity, IT: Immunotoxicity; SS: Skin Sensitization.

of **E38** and **E40** molecules complexed with M^{Pro}. To set up the simulation, initially, the systems were built for complexes of **E38**-M^{Pro} and **E40**-M^{Pro}, respectively, in a system builder. For this purpose, Desmond 2018-4 was used to set up the initial parameters within an explicit SPC water model and placed in the orthorhombic box 4.0 × 4.0 × 4.0 Å. All the protease-ligand complexes were neutralized with NaCl by adding 0.15 M Na⁺ ions. ASL module was used to select the

specific residues of ligand and protein molecule. The prepared systems were relaxed using Desmond default protocol of relaxation (Khan et al., 2020). MDS run of 20 ns was set up at constant temperature and constant pressure (NPT) for the final production run. The NPT ensemble was set up using Nosé–Hoover chain coupling scheme (Dayer et al., 2017) at temperature 300 K for final production and throughout the dynamics with relaxation time 1 ps. RESPA integrator was used to calculate the binding interactions for a time step 2 fs (Kaiser, 2005). All the other parameters were associated in the settings as described elsewhere (Chowdhury, 2020). After the final production run, the simulation trajectories of main protease complexed with **E38** and **E40** molecules were analyzed for final outcome of RMSD, RMSF and number of hydrogen bonds formed from the simulation. Binding energies of the complexes were calculated using MM-GBSA (Genheden & Ryde, 2015) for every 1 ns trajectory up to 20 ns and the average binding energies with standard deviations were measured for accurate binding approximation and stability described elsewhere (Genheden & Ryde, 2015).

3. Results and discussion

3.1. *In silico* pharmacokinetic and ADMET assays

In silico screening of compounds against new coronavirus targets is considered a useful strategy for the detection of molecules with great probability of presenting good pharmacokinetic properties and *in vitro* and *in vivo* low toxicity (Yang et al., 2020). Thus, we used *in silico* approaches to predict the pharmacokinetics and the toxicological potential of 101 phthalimide-1,2,3-triazole derivatives, aiming to identify leader compounds against SARS-CoV-2 (Figure 1). These compounds were categorized according to the radicals attached to the 1,2,3-triazole-phthalimide nucleus into groups A–H, as showed in supplementary material (Tables S1–S8): (A) derivatives containing benzyl substituents (Tehrani et al., 2019); (B) derivatives containing phenyl or benzothiazole groups (Da Silva et al., 2019); (C) derivatives containing carbohydrate groups and an additional phthalimide (Assis et al., 2012); (D) compounds with *N*-phenylacetamides substituents (Phatak et al., 2019); (E) presence of benzimidazole group between phthalimide-triazole nucleus and three radicals variations (Singh et al., 2020); (F) thalidomide derivative analogues (Ronnebaum & Luzzio, 2016); (G) derivatives of phthalimide-benzamide-1,2,3-triazole (Sadat-Ebrahimi et al., 2020); and (H) derivatives with an additional phthalimide (López-González et al., 2016).

For hit compounds selection, molecules from the above-mentioned series, that violated the Lipinski's rule of five (RO5) and therefore, those which have poor druglike properties, were filtered out. The lipophilicity and solubility are the key molecular properties for drug absorption. Lipinski's rule of five is a rule of thumb that describes the druggability of a given molecule. Our pharmacokinetic analysis (supplementary material, Tables S9 and S10) revealed that 44 out 101 compounds violated at least one of the Lipinski's rules. Out of these, 11 derivatives were predicted to have low gastrointestinal absorption (GIA). Although the compounds **B03** and **B04**

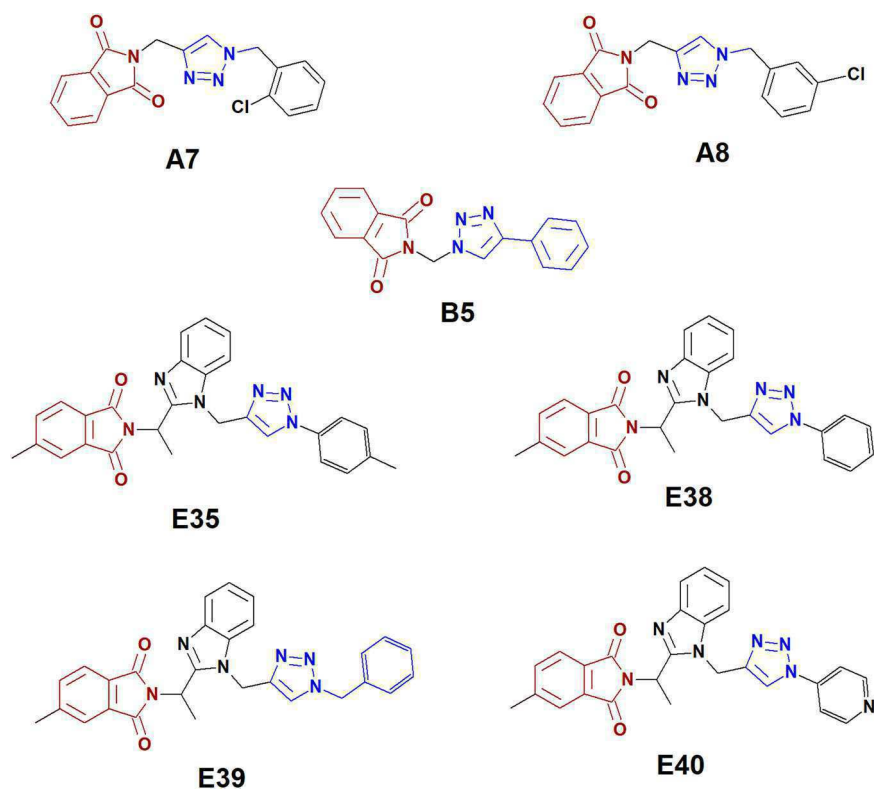


Figure 2. The chemical structures of derivatives A7, A8, B5, E35, E38, E39, and E40 chosen for molecular docking studies.

Table 3. iGemDock predictive profile of binding energies for A07, A08, B05, B35, E38, E39 and E40 triazole-phthalimide derivatives against SARS-CoV-2 targets.

Comp.	Energy (kcal/mol)	M ^{pro} 5R80	Spike protein				NCP 6VYO
			6VSB	6VXX	6VYB		
A07	E	-103.8	-94.83	-92	-89.47	-94.5	
	VDW	-95.41	-71.12	-79.44	-74.98	-80.5	
	HB	-8.4	-23.71	-12.56	-14.5	-14	
	Elec	0	0	0	0	0	
A08	E	-103.4	-93.35	-91.74	-101.5	-94.5	
	VDW	-95.32	-83.81	-84.52	-86.46	-80.5	
	HB	-8.1	-9.54	-7.22	-15.1	-14	
	Elec	0	0	0	0	0	
B05	E	-89.9	-99.48	-107.5	-84.81	-88.18	
	VDW	-79.51	-66.62	-76.07	-67.26	-75.4	
	HB	-10.4	-32.86	-31.48	-17.55	-12.7	
	Elec	0	0	0	0	0	
E35	E	-107.5	-98.8	-102.2	-109.1	-102.5	
	VDW	-95.5	-78.2	-92.48	-91.94	-92.9	
	HB	-12	-26.59	-9.80	-17.24	-9.6	
	Elec	0	0	0	0	0	
E38	E	-117.2	-107.1	-116.6	-93.2	-105.3	
	VDW	-109.1	-91.53	-94.08	-80.36	-87.3	
	HB	-8.1	-15.61	-22.61	-12.84	-18	
	Elec	0	0	0	0	0	
E39	E	-103.3	-99.32	-108.4	-98.55	-108.8	
	VDW	-99.3	-83.36	-91.46	-90.85	-91.8	
	HB	-4	-15.96	-16.94	-7.7	-17	
	Elec	0	0	0	0	0	
E40	E	-106.3	-105.1	-94.82	-96.75	-101.9	
	VDW	-99.36	-82.52	-91.02	-87.53	-89.4	
	HB	-7	-22.65	-3.8	-9.21	-12.5	
	Elec	0	0	0	0	0	

E: energy; VDW: van der Waals; HB: hydrogen-bond; Elec: electrostatic interactions.

did not violate the RO5, they showed a low GIA profile and were also rejected as hit compounds. Thus, 57 compounds were further submitted to ADMET analysis (Table 1).

The high oral bioavailability, preconized by Lipinski's rules, is one of main desirable characteristics of a druggable compound and an important factor for the optimization of bio-active molecules as therapeutic agents. Oral route is one of the preferred pathways of drug administration due to its unique advantages, including sustained and controllable drug delivery, easy administration and high patient compliance (Ekins et al., 2010; Homayun et al., 2019). Passive intestinal absorption (associated with low MW), reduced molecular flexibility (measured by NRB), low TPSA or total hydrogen bond counts (HBA and HBD) are important predictors of good oral bioavailability (Brito, 2011). A compound having CLogP ranging 0.5 to 3.5 and molecular mass < 500 kDa is considered a druggable candidate (Tetko et al., 2016).

The presence of more than two heterocycles groups in the same molecule can result in compounds with high molecular weight and LogP values. These characteristics can be observed in most of the compounds belonging to the group E (1,2,3-triazole-benzimidazole-phthalimide derivatives) and in compounds G07 and G08 (1,2,3-triazol-benzamide-phthalimide), which are therefore excluded from our study. Independently of molecular weight, compounds with high probability of good oral bioavailability have no more than 5 hydrogen bond donors and no more than 10 hydrogen bond acceptors. According to these latter criteria, our predictive analysis showed that the C03 and C02, D05, G09, G10, and G11 have low permeability throughout biological barriers.

The blood-brain barrier (BBB) protects the central nervous system (CNS) preventing certain substances (mostly harmful) from entering the brain tissues. The BBB limits the passage

of most of the external compounds to maintain CNS at a steady state (Durán-Iturbide et al., 2020; Miao et al., 2019). In addition, P-glycoprotein (P-gp) actively transports a wide variety of compounds out of cells. This protein is highly associated with the ADMET properties, playing a major role in the multidrug resistance (MDR) phenomenon (Li et al., 2014). Our ADMET analysis showed that 15 out of 57 compounds are predicted to cross the BBB, and 27 compounds were identified as a potential substrate of P-gp. Total Clearance (TC) is an important parameter associated with both the half-life and bioavailability of a xenobiotic compound. This parameter has

a direct impact in determining the dose regimen (how often) and dose size (how much) of a given drug. Thus, its prediction helps us to determine the feasibility of clinical dosing and provides a framework for the starting dose in *in vivo* studies (Durán-Iturbide et al., 2020). In this work, the TC values of 1,2,3-triazoles-phthalimide derivatives varied from -0.26 to 0.85 log (mL/min/kg), for **H2** and **E37** derivatives, respectively. Higher values of TC suggest that the xenobiotic is removed rapidly from the body, whereas a low clearance value indicates slower removal.

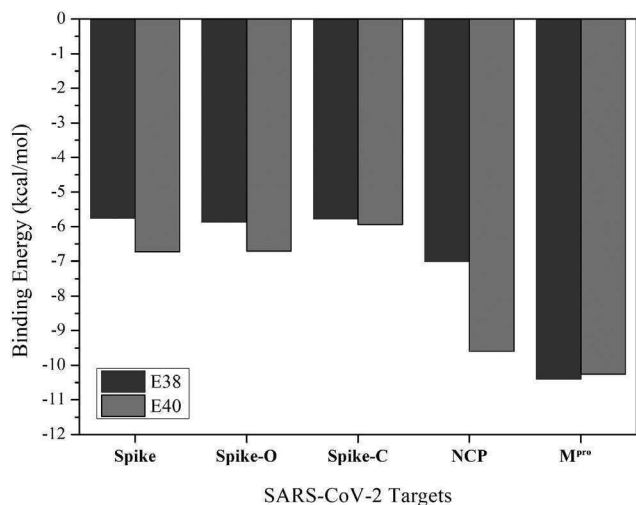


Figure 3. the graphical representation of binding energy of **E38** and **E40** derivatives on SARS-CoV-2 proteins. **Spike** (in prefusion conformation) **Spike-O**: spike protein in its open state; **Spike-C**: spike protein in its closed state; **NCP**: nucleocapsid protein; **M^{pro}**: main protease.

3.2. Prediction of toxicological potential of 1,2,3-triazole-phthalimide compounds

Poor pharmacokinetics and adverse side effects, due to compound toxicity, are pointed as the main causes of late-stage failures in drug development (Li et al., 2019). In this regard, *in silico* predicted toxicological potential of the above-mentioned compounds was investigated. Our results showed that 15 out of 57 compounds were positive for AMES and 46 compounds presented potential to be hepatotoxic. Of these, 10 compounds were both positive for AMES and hepatotoxic. The analysis of 8 selected compounds, that were either negative for AMES test or presented no hepatotoxic potential, revealed a predicted LD₅₀ for acute toxicity in rats ranging from 1,888 to 2,980 mol/kg. The minimum value for oral chronic toxicity (ORCT) was 0.160 and the maximum value was 2,046 mg/kg/day. Besides presenting positive score for AMES test and hepatotoxicity the compound **A09** also showed potential to cause adverse effects on the skin (Table 2).

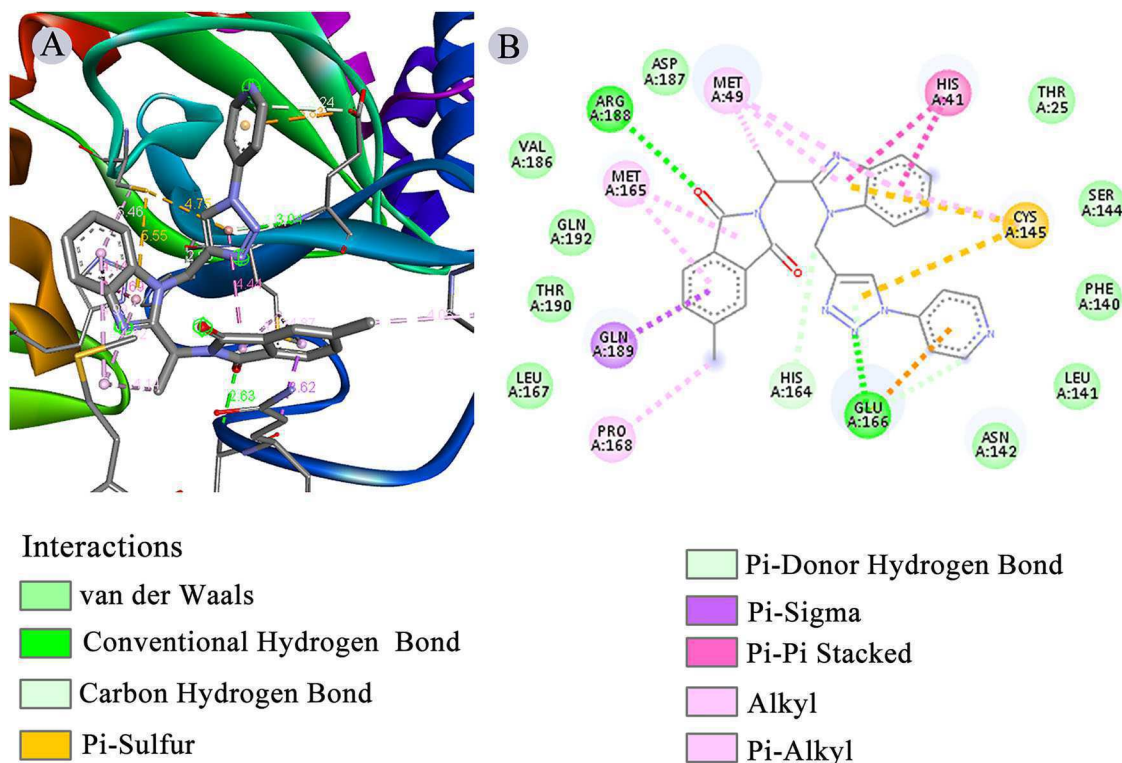


Figure 4. The molecular docking of derivative **E40** with **M^{pro}**. (A) Representative diagram of docking result of **E40** with **M^{pro}**. (B) Binding interaction of **E40** with amino acid residues of **M^{pro}**.

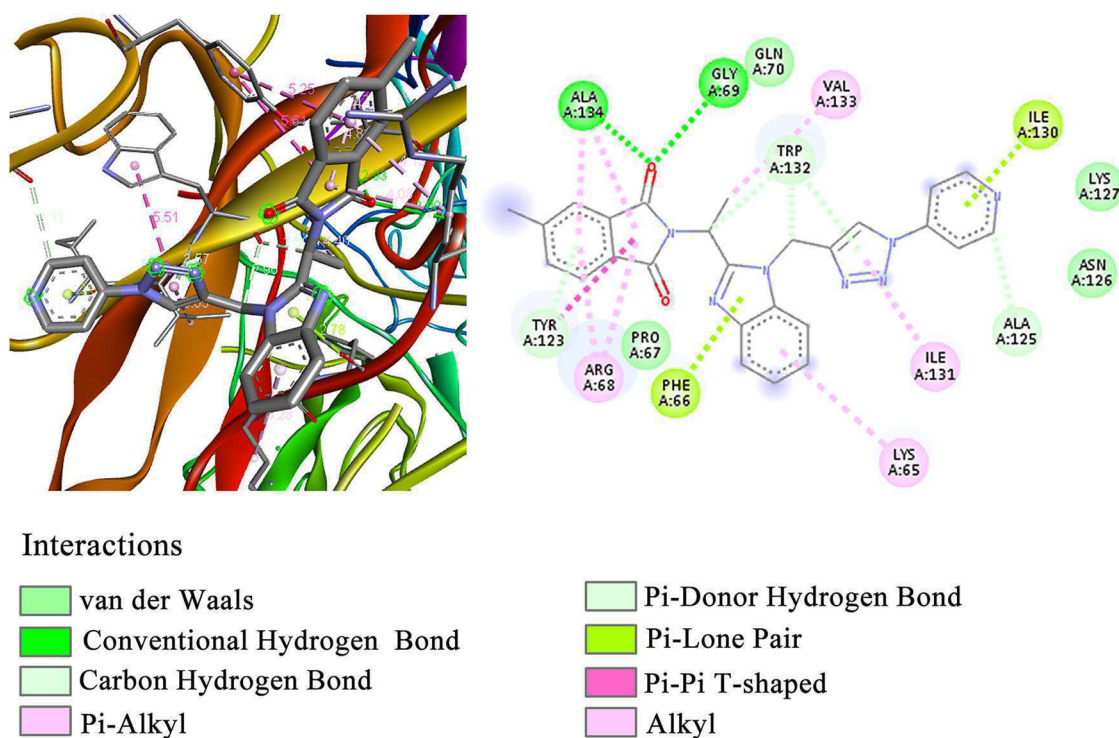


Figure 5. The molecular docking of derivative E40 with NCP. (A) Representative diagram of docking result of E40 with NCP. (B) Binding interaction of E40 with amino acid residues of NCP.

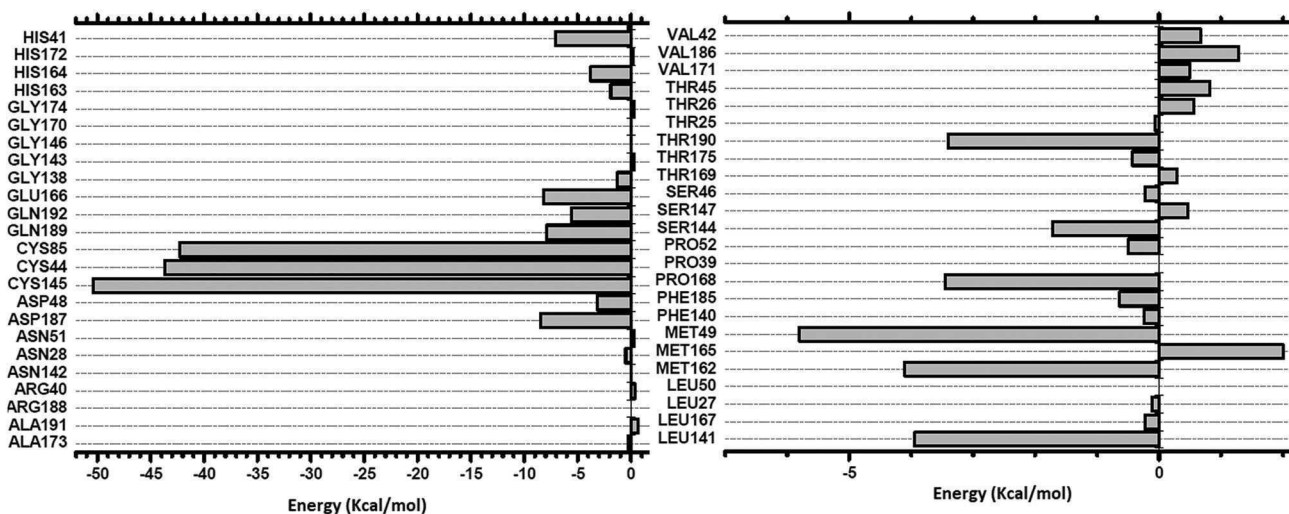


Figure 6. Energy for each nucleocapsid phosphoprotein amino acids in a radius of 15 Å from E40 ligand.

In silico predictive toxicological evaluation is easy to perform, cost-effective, high-throughput alternative to *in vitro* assays and, even replaces time-consuming, expensive *in vivo* experiments (Myatt et al., 2018). Derivatives **E26**, **E27**, **E31**, **E33**, and **E37** showed a positive predictive result for the AMES test, a method that assesses the mutagenic potential of chemical compounds (Kauffmann et al., 2020). The absence of a methyl at the carbon 5 of phthalimide ring and the presence of 1H-benzo[d]imidazole group may be related to the toxic effect of these compounds. In addition, changes in benzimidazole ligands can modulate their binding to deoxyribonucleic acid and the selectivity of these

compounds towards the host genetic material (Gümüş et al., 2009).

Besides the mutagenic potential, another important variable taken in account in our predictive analysis was the evaluation of the hepatotoxic potential of selected phthalimide-1,2,3-triazole derivatives. Although the compounds **A01**, **A02**, **A04**, **A06**, **A09**, **A10**, **A11** and **A12**, that have phthalimide-1,2,3-triazol-phenyl as the main structural group, were negative for AMES test, they showed important hepatotoxic potential. The presence of the methyl-benzyl group linked to 1,2,3-triazole-phthalimide nucleus, as well as the insertion of binders such as fluorine and bromine, may be

related to the deleterious potential of these compounds. Interestingly, the compounds from the same series that did not show a predictive hepatotoxic effect, contained chlorine at the carbon 2 or 3 of phenyl group. However, this same result was not observed when 2,3-dichloro or 3,4-dichloro was present. Like the derivatives from the **A** series, the molecules **E25**, **E45**, **G05**, and **G07** that also presented predictive hepatotoxic potential, have substituted halogenated groups in their structures. In order to better understand the

Table 4. Interaction energies between RNA binding domain of nucleocapsid phosphoprotein residues and **E40**.

Amino acids	Energy
ASP63	5.00
LEU64	6.10
LYS65	-7.00
PHE66	-4.32
PRO67	0.00
ARG68	-5.89
GLY69	-8.89
GLN70	-4.43
GLY71	-8.12
VAL72	-0.52
ILE84	-0.33
GLY85	-33.74
TYR86	-31.00
TYR87	-24.50
LEU121	-28.65
PRO122	-24.55
TYR123	-21.63
GLY124	-14.20
ALA125	-1.22
ASN126	-1.31
GLY129	-2.01
ILE130	-2.14
ILE131	1.87
TRP132	2.01
VAL133	2.02
ALA134	4.31
THR135	3.22
GLU136	4.87
ALA138	1.51
THR166	6.90
Total energy	-1.87E + 2 kcal/mol -8.03 eV

Table 5. Interaction energies between Spike-O amino acid residues and **E40**.

Amino acids	Energy
LYS1038	2.87
PHE906	-3.51
ASN907	-4.85
GLY908	0.31
ILE909	0.11
GLY910	0.20
VAL911	0.02
THR912	0.17
GLN1036	-2.14
SER1037	-22.17
LYS1038	-31.89
VAL1040	-15.72
ASP1041	-11.59
CYS1043	-9.25
GLY1046	-5.78
TYR1047	-5.23
HIS1048	-4.17
LEU1049	-10.83
THR1066	-4.22
TYR1067	-4.82
VAL1068	-10.11
GLU1092	-7.05
GLY1093	-4.04
GLN1106	4.58
ARG1107	2.89
ASN1108	-5.13
GLY885	-5.01
TRP886	-3.54
THR887	-0.17
GLY889	-5.12
ALA890	-3.21
GLN901	-3.71
ALA903	-2.63
TYR904	-1.72
ARG905	-2.47
ASN907	-18.12
GLY908	-2.14
ILE909	5.21
GLY910	5.87
GLU1031	3.17
GLY1035	3.16
GLN1036	-2.51
SER1037	-8.10
LYS1038	17.54
HIS1048	-5.81
Total energy	-1.81E + 02 kcal/mol -7.77 eV

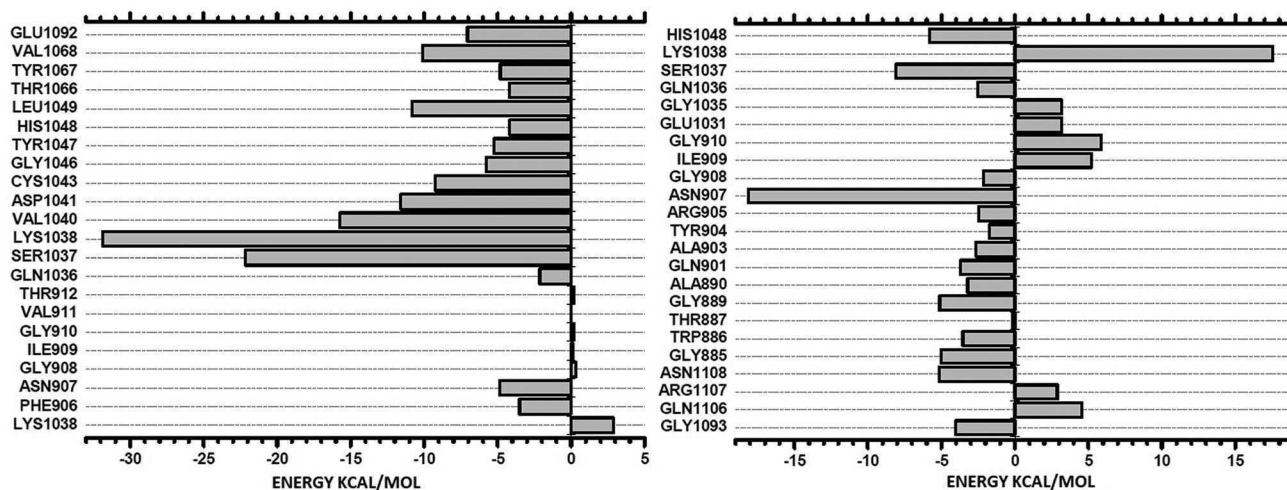


Figure 7. Energy for each Spike-O amino acids in a radius of 15 Å from **E40** ligand.

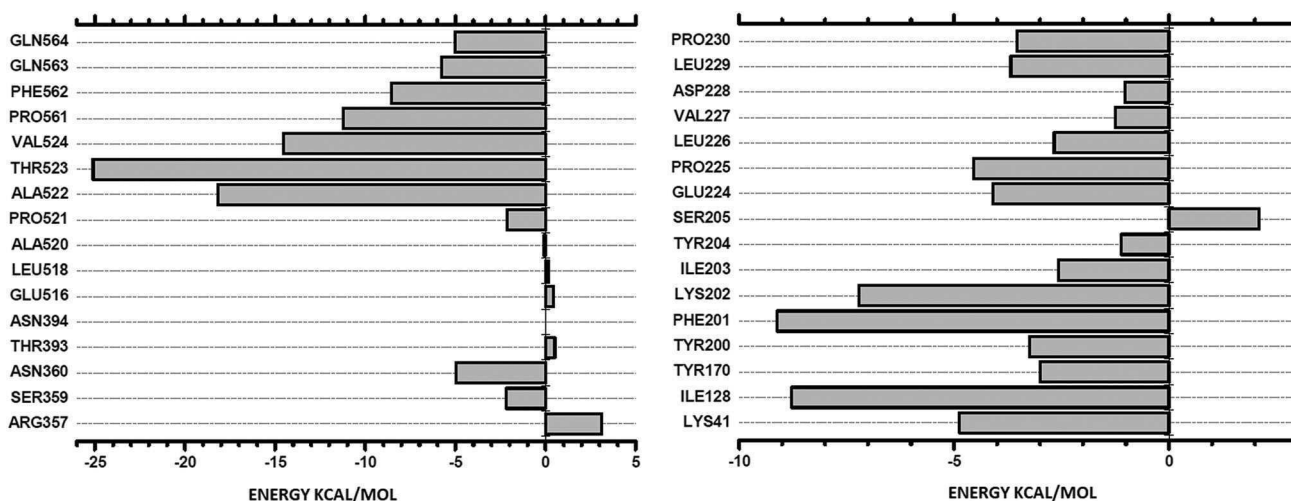


Figure 8. Energy for each Spike-C amino acid in a radius of 15 Å from E40 ligand.

Table 6. Interaction energies between Spike-C amino acid residues and E40.

Amino acid	Energy
ARG357	3.12
SER359	-2.18
ASN360	-4.97
THR393	0.52
ASN394	0.00
GLU516	0.44
LEU518	0.17
ALA520	-0.07
PRO521	-2.13
ALA522	-18.18
THR523	-25.10
VAL524	-14.56
PRO561	-11.20
PHE562	-8.56
GLN563	-5.77
GLN564	-5.01
LYS41	-4.87
ILE128	-8.78
TYR170	-2.99
TYR200	-3.25
PHE201	-9.11
LYS202	-7.21
ILE203	-2.56
TYR204	-1.11
SER205	2.10
GLU224	-4.10
PRO225	-4.55
LEU226	-2.67
VAL227	-1.25
ASP228	-1.02
LEU229	-3.68
PRO230	-3.53
Total energy	-1.52E +02 kcal/mol -6.54 eV

structure-toxicity relationship of the compounds containing halogen atoms, further evaluation of other chemical-structural parameters is required (Kortagere et al., 2008).

The derivatives **B01**, **B02**, **B06**, **B07**, and **B08** also showed positive predictive results for hepatotoxicity. The difference in the number of carbons in the aliphatic chain between phthalimide and triazole, also present in the molecules **C04**, **C05** and **C06**, **H01** and **H02**, could explain, at least in part, the predicted hepatotoxic potential found for compounds belonging to this series. Consistently, the number of carbons present in the aliphatic chain, that joins pharmacophoric

groups in hybrid derivatives of 1,2,3-triazole-phthalimide, has been associated with the occurrence *in vivo* hepatotoxicity (Da Silva et al., 2019). The presence of the benzothiazole group in compounds of the **E** series did not appear to be determinant for the predicted hepatotoxicity of these molecules, since other triazole-phthalimide derivatives containing the same group, like **E26**, **E27**, **E38**, **E31** and **E33** did not present hepatotoxic potential. Heterocyclic molecules containing the benzothiazole group have shown to be more promising drug candidates to treat infectious diseases, reinforcing the pharmacological potential of benzothiazole-containing molecules (Papadopoulou et al., 2013). It has been reported that molecules containing thalidomide group in its structure, as those of series **F**, presented high hepatotoxic potential (Kamiya et al., 2020). In this regard, only the derivatives **A7**, **A8**, **B5**, **E35**, **E38**, **E39**, and **E40** (Figure 2) showed good pharmacokinetic and toxicological profiles, and were therefore chosen for molecular docking.

3.3. Molecular docking of selected 1,2,3-triazole-phthalimide compounds

Computational simulations of ligand-protein docking are an important component of drug discovery, being mainly used for the virtual screening of hit compounds from large databases and to identify and evaluate the effects of chemical changes during leader optimization (Bordogna et al., 2011). In this regard, the accuracy of modeled structures should be taken into account. Our stereochemical analysis of SAR-CoV-2 target proteins, obtained from PDB (Figures S1–S5), showed that the percentage of the sum of amino acid residues in the most favoured and additional allowed regions was $\geq 95\%$. This result confirmed the high quality of our selected target models (Laskowski et al., 2006). In order to validate our molecular docking, the co-crystal standard ligand (RGZ, methyl 4-sulfamoylbenzoate) of M^{PrO} complex (5R80) was redocked against this protein and the root-mean-square deviation (RMSD) was calculated for predicting the stability of the protein and protein-ligand complexes. Our results showed that Autodock program was able to generate a

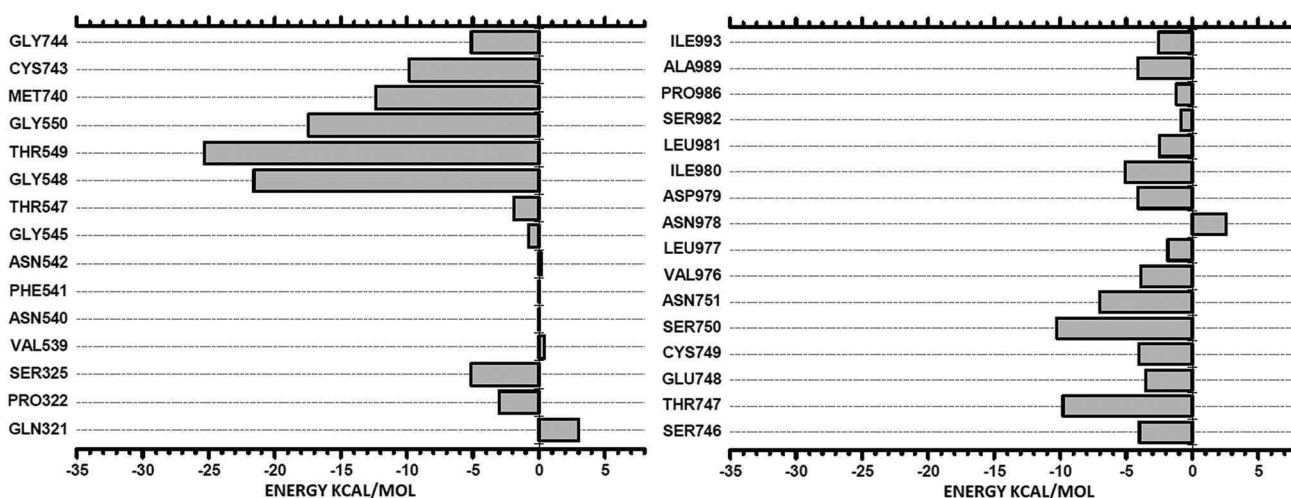


Figure 9. Energy for each spike glycoprotein (with a single receptor-binding domain up) amino acids in a radius of 15 Å from E40 ligand.

Table 7. Interaction energies between spike glycoprotein (with a single receptor-binding domain up) residues and E40.

Amino acids	Energy
GLN321	3.01
PRO322	-3.02
SER325	-5.13
VAL539	0.43
ASN540	0.01
PHE541	0.05
ASN542	0.18
GLY545	-0.78
THR547	-1.89
GLY548	-21.58
THR549	-25.31
GLY550	-17.44
MET740	-12.37
CYS743	-9.81
GLY744	-5.11
ASP745	-5.12
SER746	-4.01
THR747	-9.78
GLU748	-3.55
CYS749	-4.02
SER750	-10.24
ASN751	-7.03
VAL976	-3.89
LEU977	-1.85
ASN978	2.54
ASP979	-4.12
ILE980	-5.08
LEU981	-2.50
SER982	-0.84
PRO986	-1.22
ALA989	-4.10
ILE993	-2.56
Total energy	-1.66E +02 kcal/mol -7.14 eV

successful pose (RMSD = 1.9 Å) (Figure S6). It is assumed that scored poses with an RMSD of less 2.0 Å are considered to be successful (Bordogna et al., 2011; Razzaghi-Asl et al., 2020).

The docking analysis using iGemDock software revealed that the derivatives **A7**, **A8**, **B5**, **E35**, **E38**, **E39**, and **E40** showed favourable interactions energies for all the tested proteins from SARS-CoV-2 (Table 3). **E38** presented higher binding energy valued for spike protein in its closed state (Spike-C) (-116.6 kcal/mol) and spike protein in prefusion conformation (-107.1 kcal/mol). The higher binding energy

value for main protease (M^{Pro}) was found for its interaction with **E38** (-117.2 kcal/mol). Among the tested compounds, **E39** presented highest affinity to RNA binding domain of nucleocapsid phosphoprotein with binding energy of -108.8 kcal/mol. For all ligand-protein complexes, the interaction energies were predominantly due to Van der Waals, followed by hydrogen bonds. No electrostatic interactions were observed for all interactions of compounds with SARS-CoV-2 proteins.

The use of molecular docking has been largely applied as a strategy for the selection of possible leader candidates against the new coronavirus (Karypidou et al., 2018). Since the SARS-CoV outbreak in 2002, *in silico* molecular docking and structural studies have demonstrated a relationship between the SARS-CoV-2 spike receptor-binding domain and the angiotensin-2 receptor (ACE2) in the host cells. This association is strictly linked to the infection and transmission of new corona virus in humans (Utomo & Meiyanto, 2020). The wide distribution of the ACE2 receptor in human tissues and organs could be related to the appearance of symptoms in the severe phase of the disease, mainly in the pulmonary system, where it is largely expressed at the surface of type II alveolar cells (Sanchis-Gomar et al., 2020). In our analysis we docked the selected compounds on different conformational states of SARS-CoV-2 spike protein. Overall, our results showed that all the selected compounds bound with high affinity to spike proteins independently of its conformational state (open, close, or in prefusion conformation). However, slight differences in binding energy values were observed. The lowest binding energy value found for the interaction of **E38**, and **E35** derivatives with different conformational states of spike protein, revealed the binding plasticity of 1,2,3-triazole-phthalimide derivatives towards this protein. Liu et al. (2004) described that the inhibition of peptides in the heptad repeat regions of the SARS-CoV spike protein results in the interference of the fusogenic mechanism. In this regard, it is possible that the selected Top-7 derivatives may interfere with the SARS-CoV-2 binding, entrance and replication processes in the host cells.

The predictive analysis of the inhibition constant values for best binding pose of protein-ligand complexes was

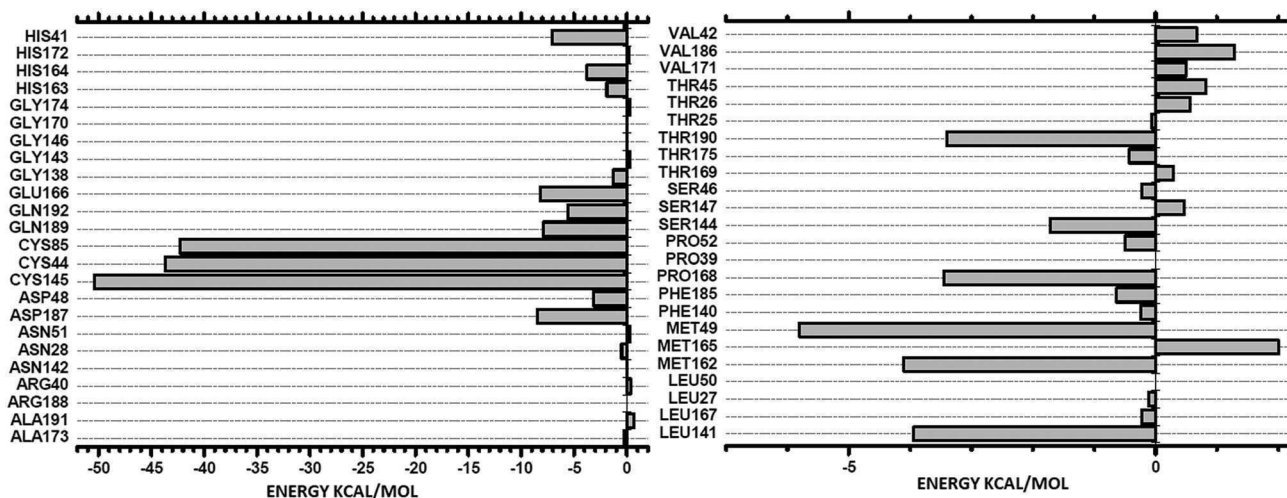


Figure 10. Energy for each main protease amino acids in a radius of 15 Å from E40 ligand.

Table 8. Interaction energies between main protease amino acid residues and E40.

Amino acids	Energy
ALA173	-0.25
ALA191	0.69
ARG188	0.00
ARG40	0.41
ASN142	0.02
ASN28	-0.50
ASN51	0.29
ASP187	-8.47
ASP48	-3.15
CYS145	-50.42
CYS44	-43.68
CYS85	-42.31
GLN189	-7.90
GLN192	-5.54
GLU166	-8.19
GLY138	-1.28
GLY143	0.26
GLY146	0.01
GLY170	0.03
GLY174	0.31
HIS163	-1.89
HIS164	-3.78
HIS172	0.23
HIS41	-7.06
ILE43	-0.22
LEU141	-3.94
LEU167	-0.23
LEU27	-0.11
LEU50	0.00
MET162	-4.10
MET165	2.00
MET49	-5.80
PHE140	-0.24
PHE185	-0.64
PRO168	-3.45
PRO39	0.00
PRO52	-0.50
SER144	-1.71
SER147	0.47
SER46	-0.23
THR169	0.29
THR175	-0.43
THR190	-3.40
THR25	-0.06
THR26	0.56
THR45	0.82
VAL171	0.50
VAL186	1.28
VAL42	0.67
Total energy	-2.01E +02 kcal/mol -8.63 eV

performed using AutoDock software (Tables S11–S17). Our results showed that **A7**, **E35**, **E38** and **E40** presented higher binding affinity for at least one of the viral target SARS-CoV-2 proteins, with inhibition constant values (K_i) in the nanomolar range. All of these compounds showed high affinity for SARS-CoV-2 main protease. Comparing all ligand-protein interactions tested, the lowest values of inhibition constant (K_i) were found for the interaction of the compound **E38** with M^{pro} with $K_i = 23.85$ nM and binding energy of -10.4 kcal/mol for the best pose. The second-best value of K_i was obtained for the **E40**- M^{pro} complex with $K_i = 30.04$ nM and a binding energy of -10.26 kcal/mol. Compound **E40** also bound with high affinity to nucleocapsid protein, with $K_i = 91.09$ nM and binding energy of -9.6 kcal/mol (Figure 3).

In addition to the spike protein, coronavirus proteases are also essential for viral transmission and virulence by processing viral proteins involved in viral replication (Báez-Santos et al., 2015). Compounds that act as inhibitors of these proteins can be considered as promising antiviral agents by reducing the severity of the infection (Hall & Ji, 2020). All the top-7 compounds bound with high affinity to SARS-CoV-2 main protease, being **E38** and **E40** the compounds that presented the highest affinity (i.e. the lowest binding energy) towards this target. The analogous performance of these compounds toward M^{pro} can be attributed to chemical-structural similarities of the two derivatives, which are only distinguished from each other by the presence of the phenyl and pyridin-4-yl groups in the N1 of triazole ring. Molecules containing 1,2,3-triazole group have already been described as having anti-coronavirus activity, by interacting with viral proteases, corroborating the relevance of these proteins as the main target of these compounds (Karypidou et al., 2018). The main amino acids involved in **E40**-SARS-CoV-2 binding were MET165, MET49, HIS41, CYS145, GLU166 and GLN189 (M^{pro} —Figure 4) and ALA134, GLY69, VAL133, TRP132, ILE130, ALA125, ILE131, LYS65, PHE66, ARG68 and TYR123 (NCP—Figure 5). The most prevalent interaction was Van der Waals and hydrogen bonds. The electrostatic binding energy values were insignificant when compared to the contributions of van der Waals and hydrogen bonds.

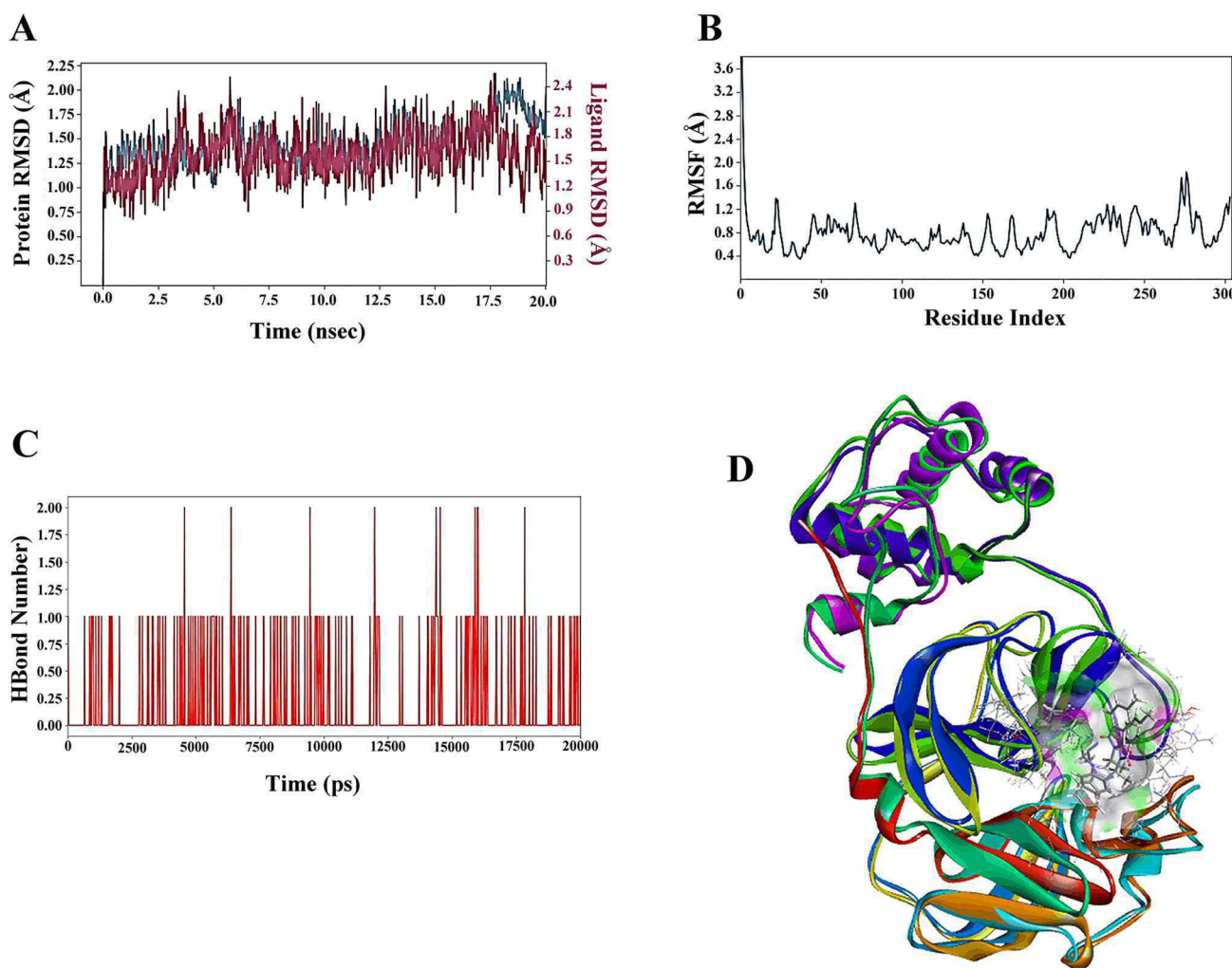


Figure 11. The molecular dynamic (MD) simulations of main protease bound to **E38**. (a) RMSD plot of C α -backbone (blue) and ligand (red) displayed stable convergence till 20 ns. (b) RMSF plot depicting fluctuations of each residual position of main protease amino acids. (c) Number of H-bonds formed during the entire course of simulation. (d) Superimposed initial and final frame structures of main protease complexed with **E38** (surface view) molecule before and after simulation.

In this study we also docked the Top-7 1,2,3-triazole-phthalimide derivatives on viral nucleocapsid protein. NCPs have been considered strategic targets to fight acute respiratory infections caused by SARS-CoV-2 due to their multiple functions in the viral replication cycle (Kang et al., 2020). All the compounds tested bound with high efficiency on NCP. Comparing the best-pose of selected molecules (1/10) for the NCP, the **E40** presented the most favorable binding energy (-9.6 kcal/mol) and was the only one that achieved an inhibition constant in the nanomolar range for this target. The interaction of these compounds with nucleocapsid proteins may interfere with essential functions of the viral cycle, such as the formation of the helical ribonucleoprotein complex, during the packaging of the viral genome, and the control of basic cellular functions in the host cell, like the deregulation of the cell cycle (Cong et al., 2020; Surjit et al., 2006). Although further *in vitro* analysis are needed to better understand the biological effects of the interaction of **E40**-SARS-CoV-2 nucleocapsid proteins complex, the high predicted binding affinity of this compound to these proteins suggests that **E40** may prevent nucleocapsid proteins from participating in the replication and release of viral particles (Zeng et al., 2008).

A characteristic of RNA viruses is the high rate of genetic mutation, which can result in the evolution of new viral strains and the inefficacy of treatment. Therefore, from a public-health perspective, the ability of our top-7 selected 1,2,3-triazole-phthalimide derivatives to bind to different viral proteins, may circumvent the drug resistance caused by single-target mutations or rare simultaneous mutations of several targets in different positions (Xu et al., 2020). Although some compounds were excluded from our study, it is important to take in mind that these molecules can be redesigned for more rational chemical-structural modifications, decreasing its toxic potential and/or improving their biological activity against target molecules.

Because our molecular docking analysis has pointed the compound **E40** as the most promising compound, the best complexes obtained between this compound and the targets were subjected to quantum energy calculations by the MFCC technique. The results of the interactions between **E40** and amino acids of the RNA binding domain of nucleocapsid phosphoprotein (PDB-ID 6VYO) are described in Figure 6 and Table 4.

Overall, 30 amino acids of NCP showed some kind of interaction with **E40**, 11 showing repulsion and 19 attraction

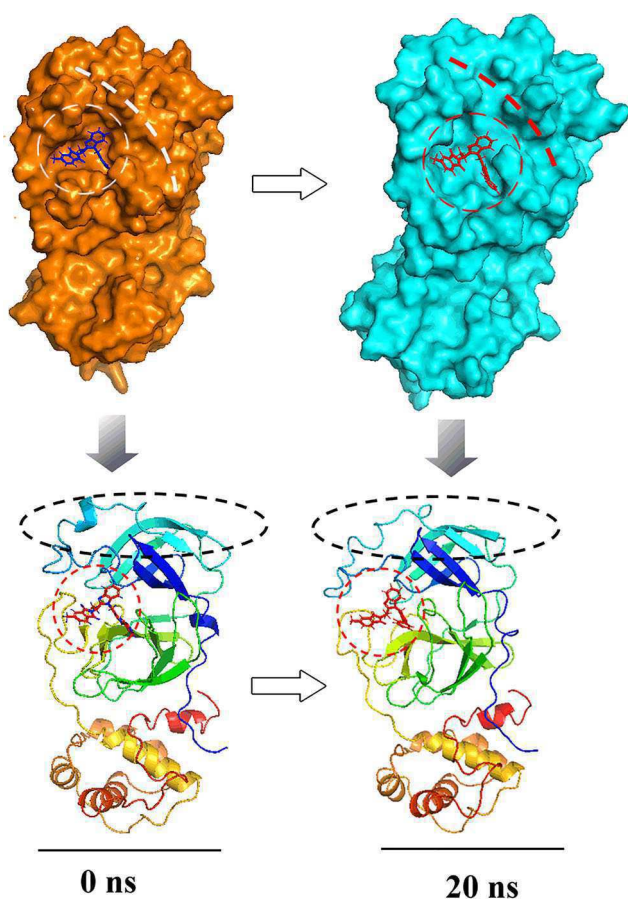


Figure 12: Surface view of main protease before MD simulation (orange) displaying little modifications in the E38-M^{Pro} binding site (yellow ring) after simulation (cyan teal). Lower panel depicted the conformational differences between the structures of E38 in the binding site provided orientation that is more accurate for higher binding.

with the ligand. The PRO67 residue presented energy value of 0.00. Consequently, it cannot be confirmed whether the interaction occurring with the ligand is repulsive or attractive. The general energy balance points to a stronger attraction (-8.03 eV) between the connection site of protein and the E40 compound. The residues GLY85, TYR86, TYR87, LEU121, PRO122, TYR123 and GLY124 presented very low energies (negative values), suggesting very strong attractions by these amino acids, which are probably the anchor residues. Figure 7 and Table 5 show MFCC results between E40 and the open state of SARS-CoV-2 spike ectodomain structure (PDB-ID 6VYB).

A total of 45 residues of spike-O showed energetic interactions with the drug, 13 of which are interacting repulsively and 32 attractively. The residues VAL1040, ASP1041, LEU1049, VAL1068, ASN907, and LYS1038 demonstrated a strong attraction for the ligand, possibly acting as anchoring residues. Figure 8 and Table 6 describe the results of the MFCC for interactions between spike glycoprotein in closed state (PDB-ID 6VXX) and E40.

There were 32 amino acids of spike protein interacting with E40, 5 with positive energies (repulsion), 26 with negative energies (attraction) and one with 0.0 energy (ASN394). The amino acids that stood out for having a strong attraction were: ALA522, THR523, VAL524 and PRO561. Although the

structures obtained at inputs spike-C and spike-O represented different conformational states of the same structural protein of SARS-CoV-2 (spike glycoprotein), the compound E40 was strongly attached to both conformations but in different places. The results obtained for spike glycoprotein with a single receptor-binding domain up (6VSB) are shown in Figure 9 and Table 7.

A total of 32 residues of spike glycoprotein (with a single receptor-binding domain up) residues, interacted with the E40 ligand, 6 of which presenting repulsion and 26 attraction interactions, with emphasis on the amino acids GLY548, THR549, GLY550, MET740 and SER750, which showed strong attraction for the compound. Figure 10 and Table 8 showed the MFCC results for E40 interactions with the main protease in complex.

There are 49 amino acids of spike glycoprotein (with a single receptor-binding domain up) residues interacting with E40, 17 with slightly repulsive interactions, 3 with 0.0 energy and 29 with negative energy values. The CYS145, CYS44 and CYS85 amino acids residues, showed surprising attraction to E40, with energy values of -42.31 kcal/mol, -43.68 kcal/mol and -50.42 kcal/mol, respectively. These cysteine amino acids have already been identified as anchor residues in other studies on SARS-CoV-2 main protease (Komatsu et al., 2020). Taking in account the general energy balance, this protein also showed the lowest energy value in this study (-8.63 eV).

In a viral pandemic with rapid dispersion of cases, drug replacement strategy is promising to fight the disease, because substances that are commercially available in the pharmaceutical industry have already undergone several toxicity and safety tests. In chemistry, when atoms are held together, the energy needed to separate them is called binding energy. In covalent bonds, where the electrons are shared between atoms, the energy needed to break these bonds can vary, but energies less than -1.0 eV (Tkatchenko & Scheffler, 2009) suggest covalent bond among atoms. E40 showed lower energy values in all analyses. Interestingly, but not surprisingly, E40 showed affinity with all the three spike conformers (6VYB, 6VXX and 6VSB). Although, in this study, the ligand interacted with all Spike conformers, the anchorage residues were different in each interaction. This raises some concerns: would the E40 function as an inhibitor of the Spike-ACE2 interaction in any of the three conformers? Is there a possibility of allosteric inhibition by the E40? Although our results suggest a drug repositioning for COVID-19, further *in vivo* and *in vitro* studies are needed to answer these questions.

3.4. MD simulation and MM-GBSA binding energy calculations

The final convergence and the stability of E38 and E40 bound with the main protease was assessed by MD simulation. The analysis of RMSD and RMSF plots showed that after 20 ns of convergence, E3, bound to the main protease, displayed a significant stability (Figure 11A and 11B). The interactions of this protein with E38 displayed much less RMSD differences (~ 0.25 Å) showing its stable conformation (Figure 11A). The average of H-bonds formed between E38 and the

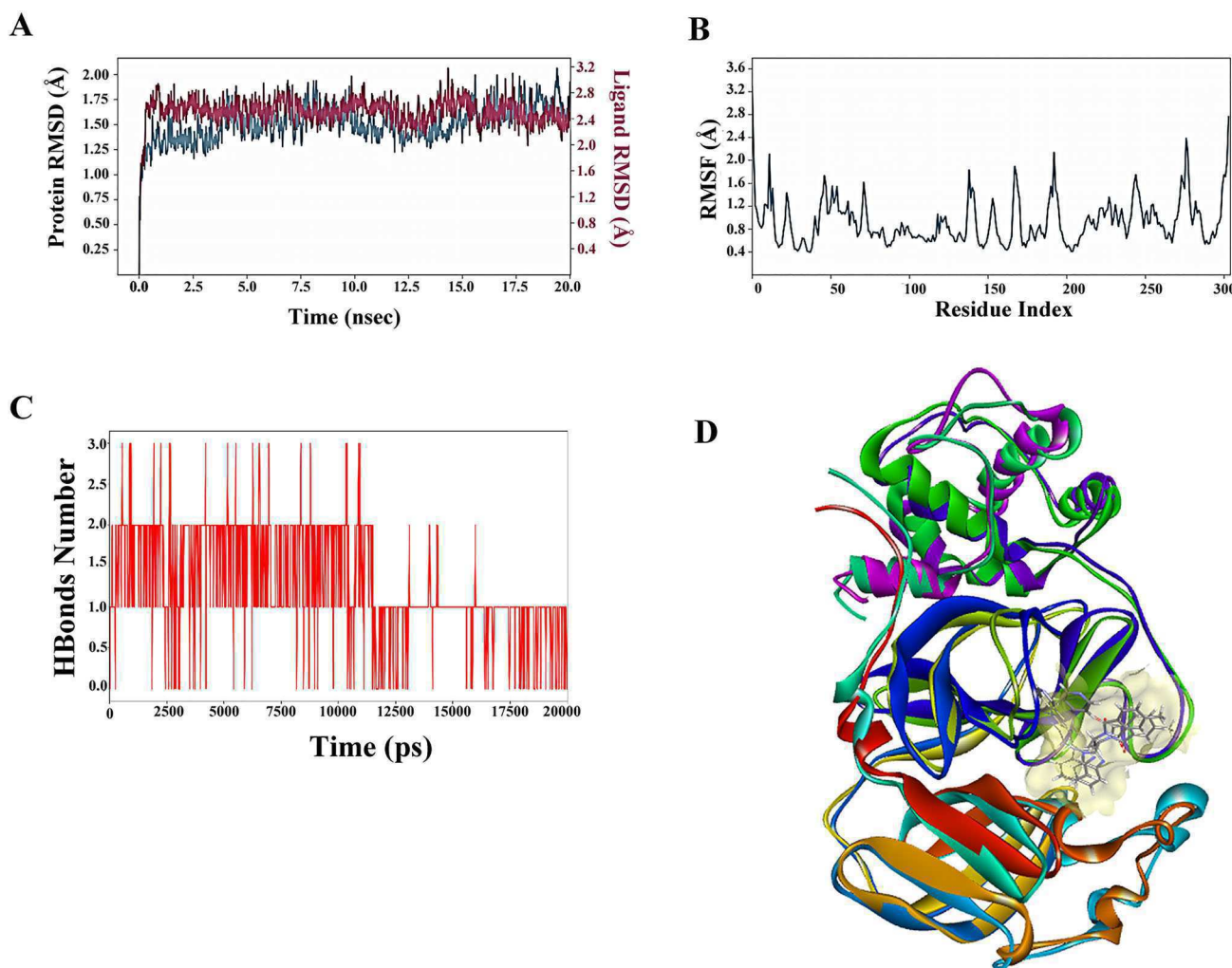


Figure 13. Molecular dynamic (MD) simulations of main protease bound to E40, (a) RMSD plot of C α -backbone (blue) and ligand (red) displayed stable convergence till 20 ns. (b) RMSF plot depicting fluctuations of each residual position of amino acids of main protease. (c) Number of H-bonds formed during the entire course of simulation. (d) Superimposed initial and final frame structures of main protease complexed with E40 (surface view) molecule before and after simulation.

main protease showed to be 1.0 throughout the simulation period for the stable conformation of both the main protease and E38 molecule (Figure 11C). The structural superimposition of the main protease-E38 complex before and after simulation displayed less significant changes in the overall conformation (Figure 11D). In addition, accommodation of E38 at the binding cavity of this protein showed small-altered orientation after simulation, which seems to be due to a change in the visible secondary structure at the E38-M^{Pro} binding site (Figure 12).

After 20 ns of convergence, the E40-M^{Pro} complex displayed significant stability as demonstrated by RMSD and RMSF plots (Figure 13A and 13B). The interactions of this protein with E40 displayed much less RMSD differences (~ 0.50 Å) conferring its stable conformation (Figure 13A). The average of H-bonds formed between E40 and the main protease showed to be 1.5 throughout the simulation period, for the stable conformation of both the main protease and the E40 molecule (Figure 13C). Structural superimposition of the main protease-E40 complex before and after simulation displayed less significant changes in the overall conformation (Figure 13D). In addition, accommodation of E40 at the binding cavity of M^{Pro} showed small-altered orientation after the simulation which

appeared to be due to the change in the visible secondary structure at the E40-M^{Pro} binding site (Figure 14).

The free energies of binding using MMGBSA were calculated for the E38 and E40-M^{Pro} complexes of SARS-CoV-2. The properties of MMGBSA calculations are displayed in Table 9. The free energy average of binding for every 1 ns trajectory up to 20 ns, for the main protease-E38 complex displayed a $dG = -63.47$ kcal/mol, with standard deviation of 3.0 kcal/mol, coulombic force of -8.70 , solvent accessibility of 20.20 and high ligand binding affinity of -1.81 . On the other hand, the E40-main protease complex displayed a $dG = -63.31$ with standard deviation of 7.0 kcal/mol and high binding efficiency, solvent accessibility and significant coulombic as well covalent energies. All the properties calculated in the MD simulation point the significant role of E38 and E40 compounds as a potent inhibitor of the main protease of SARS-CoV-2.

4. Conclusion

Taken together, our results showed that the seven selected 1,2,3-triazole-phthalimide derivatives showed an excellent

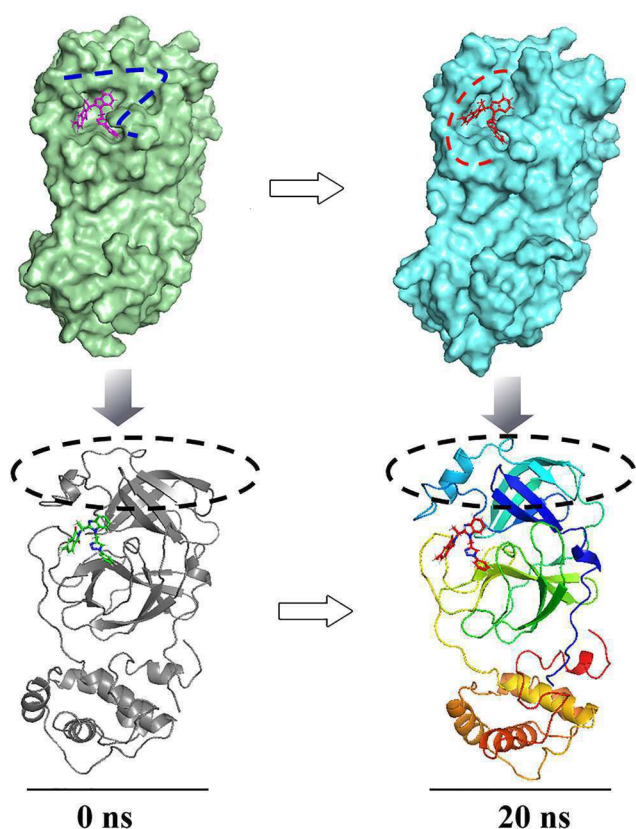


Figure 14. Surface view of main protease before MD simulation (green) displaying little modifications in the E40-M^{Pro} binding site (yellow ring) after simulation (cyan teal). Lower panel represented the conformational differences between the structures of E40 in the binding site provided orientation that is more accurate for higher binding.

Table 9. Properties calculated after MMGBSA for E38 and E40 with main protease.

Molecule	dG bind (kcal/mol)	dG coulombic force (kcal/mol)	dG covalent energy (kcal/mol)	dG solvent accessibility (Å ³)	Ligand efficiency (kcal/mol)
E38	-63.47 ± 3	-8.70	2.11	20.20	-1.81
E40	-63.31 ± 7	-15.22	1.098	25.07	-1.79

predicted pharmacokinetic and ADME properties, which are directly related to the solubility, permeability and toxicological profiles of such compounds. The *in silico* docking results showed that these selected compounds are potential multi-target ligands of essential SARS-CoV-2 spike, protease and nucleocapsid proteins suggesting the usefulness of 1,2,3-triazole-phthalimide derivatives for the development of drugs addressed to these proteins. Because the E40 presented predicted inhibition constant values in the nanomolar concentration range for both main protease and nucleocapsid proteins, this compound was considered the most promising as multi-target agent against SARS-CoV-2. Our MD simulation corroborated E40 and E38 as potent inhibitors of M^{Pro} of SARS-CoV-2. However, we cannot rule out the possibility that other compounds, such as E38 can be included in further investigations alone or in combination with E40.

Acknowledgement

Vanderlan Nogueira Holanda would like to thank Fundação de Amparo a Ciência e Tecnologia do Estado de Pernambuco (FACEPE) for the graduate scholarship (IBPG-0333-2.08/18).

Disclosure statement

The authors declare that they have no known competing financial interests or personal relationships that could have appeared to influence the work reported in this paper.

Funding

This work was supported by the Fundação de Amparo à Ciência e Tecnologia do Estado de Pernambuco (FACEPE, BFT-109-2.08/18 and BIC-0489-2.13/20) Conselho Nacional de Desenvolvimento Científico e Tecnológico (CNPq, PQ-400749/2019-0 and 312675/2018-6), Coordenação de Aperfeiçoamento de Pessoal de Nível Superior (CAPES code 001), Instituto Aggeu Magalhães and Inova-Fiocruz Program (VPPCB-007-FIO-18-2-85).

ORCID

Vanderlan Nogueira Holanda <http://orcid.org/0000-0001-5309-0036>
 Elton Marlon de Araújo Lima <http://orcid.org/0000-0003-0545-2447>
 Welson Vicente da Silva <http://orcid.org/0000-0001-5676-6863>
 Rafael Trindade Maia <http://orcid.org/0000-0002-5870-1091>
 Rafael de Lima Medeiros <http://orcid.org/0000-0003-2360-3595>
 Arabinda Ghosh <http://orcid.org/0000-0002-3891-5949>
 Vera Lúcia de Menezes Lima <http://orcid.org/0000-0003-2581-9218>
 Regina Celia Bressan Queiroz de Figueiredo <http://orcid.org/0000-0001-5806-0944>

References

- Al-Masoudi, N. A., Abood, E., Al-Maliki, Z. T., Al-Masoudi, W. A., & Pannecouque, C. (2016). Amino acid derivatives. Part 6. Synthesis, *in vitro* antiviral activity and molecular docking study of new N- α -amino acid derivatives conjugated spacer phthalimide backbone. *Medicinal Chemistry Research*, 25(11), 2578–2588. <https://doi.org/10.1007/s00044-016-1693-9>
- Assis, S. P. D. O., Silva, M. T. D., Oliveira, R. N., & Lima, V. L. D. M. (2012). Synthesis and anti-inflammatory activity of new alkyl-substituted phthalimide 1H-1,2,3-triazole derivatives. *The Scientific World Journal*, 2012, 7. <https://doi.org/10.1100/2012/925925>
- Assis, S. P. d. O., Silva, M. T. d., Silva, F. T. d., Sant'Anna, M. P., Tenório, C. M. B. d. A., Santos, C. F. B. D., Fonseca, C. S. M. d., Seabra, G., Lima, V. L. M., & Oliveira, R. N. d. (2019). Design and synthesis of triazole-phthalimide hybrids with anti-inflammatory activity. *Chemical & Pharmaceutical Bulletin*, 67(2), 96–105. <https://doi.org/10.1248/cpb.c18-00607>
- Báez-Santos, Y. M., John, S. E. S., & Mesecar, A. D. (2015). The SARS-coronavirus papain-like protease: Structure, function and inhibition by designed antiviral compounds. *Antiviral Research*, 115, 21–38. <https://doi.org/10.1016/j.antiviral.2014.12.015>
- Bhatia, R., Narang, R. K., & Rawal, R. K. (2020). A summary of viral targets and recently released PDB IDs of SARS-CoV-2. *The OpenVirology Journal*, 14, 7–8.
- Bordogna, A., Pandini, A., & Bonati, L. (2011). Predicting the accuracy of protein-ligand docking on homology models. *Journal of Computational Chemistry*, 32(1), 81–98. <https://doi.org/10.1002/jcc.21601>
- Brito, M. A. D. (2011). Pharmacokinetic study with computational tools in the medicinal chemistry course. *Brazilian Journal of Pharmaceutical*

- Sciences*, 47(4), 797–805. <https://doi.org/10.1590/S1984-82502011000400017>
- Butcher, G., Comer, J., & Avdeef, A. (2015). pKa-critical interpretations of solubility–pH profiles: PG-300995 and NSC-639829 case studies. *ADMET and DMPK*, 3(2), 131–140. <https://doi.org/10.5599/admet.3.2.182>
- Chen, Y. W., Yiu, C. P., & Wong, K. Y. (2020). Prediction of the 2019-nCoV 3C-like protease (3CLpro) structure: Virtual screening reveals velpatasvir, ledipasvir, and other drug repurposing candidates. *ChemRxiv*, 2, 2–11. <https://doi.org/10.26434/chemrxiv.11831103.v1>
- Chowdhury, P. (2020). *In silico* investigation of phytoconstituents from Indian medicinal herb *Tinospora cordifolia* (giloy) against SARS-CoV-2 (COVID-19) by molecular dynamics approach. *Journal of Biomolecular Structure and Dynamics*, 1–18. <https://doi.org/10.1080/07391102.2020.1803968>
- Cong, Y., Ulasli, M., Schepers, H., Mauthe, M., V'kovski, P., Kriegenburg, F., ... Reggiori, F. (2020). Nucleocapsid protein recruitment to replication-transcription complexes plays a crucial role in coronavirus life cycle. *Journal of Virology*, 94(4), 1–21. <https://doi.org/10.1128/JVI.01925-19>
- Dayer, M. R., Taleb-Gassabi, S., & Dayer, M. S. (2017). Lopinavir; a potent drug against coronavirus infection: Insight from molecular docking study. *Archives of Clinical Infectious Diseases*, 12(4), e13823. <https://doi.org/10.5812/archcid.13823>
- Durán-Iturbide, N. A., Díaz-Eufracio, B. I., & Medina-Franco, J. L. (2020). *In silico* ADME/Tox profiling of natural products: A focus on BIOFACQUIM. *ACS Omega*, 5(26), 16076–16084. <https://doi.org/10.1021/acsomega.0c01581> <https://doi.org/10.1021/acsomega.0c01581>
- Ekins, S., Honeycutt, J. D., & Metz, J. T. (2010). Evolving molecules using multi-objective optimization: Applying to ADME/Tox. *Drug Discovery Today*, 15(11–12), 451–460. <https://doi.org/10.1016/j.drudis.2010.04.003>
- Genheden, S., & Ryde, U. (2015). The MM/PBSA and MM/GBSA methods to estimate ligand-binding affinities. *Expert Opinion on Drug Discovery*, 10(5), 449–461. <https://doi.org/10.1517/17460441.2015.1032936>
- Gonzaga, D. T. G., da Rocha, D. R., da Silva, F. d. C., & Ferreira, V. F. (2013). Recent advances in the synthesis of new antimycobacterial agents based on the 1H-1,2,3-triazoles. *Current Topics in Medicinal Chemistry*, 13(22), 2850–2865. <https://doi.org/10.2174/15680266113136660202>
- Gümüş, F., Eren, G., Açık, L., Celebi, A., Oztürk, F., Yılmaz, S., Sagkan, R. I., Gür, S., Ozkul, A., Elmali, A., & Elerman, Y. (2009). Synthesis, cytotoxicity, and DNA interactions of new cisplatin analogues containing substituted benzimidazole ligands. *Journal of Medicinal Chemistry*, 52(5), 1345–1357. <https://doi.org/10.1021/jm8000983>
- Hall, D. C., Jr., & Ji, H. F. (2020). A search for medications to treat COVID-19 via *in silico* molecular docking models of the SARS-CoV-2 spike glycoprotein and 3CL protease. *Travel Medicine and Infectious Disease*, 35, 101646. <https://doi.org/10.1016/j.tmaid.2020.101646>
- Homayun, B., Lin, X., & Choi, H.-J. (2019). Challenges and recent progress in oral drug delivery systems for biopharmaceuticals. *Pharmaceutics*, 11(3), 129. <https://doi.org/10.3390/pharmaceutics11030129>
- Huang, C., Wang, Y., Li, X., Ren, L., Zhao, J., Hu, Y., Zhang, L., Guohui, F., Xu, J., Gu, J., Cheng, Z., Yu, T., Xia, J., Wei, Y., Wu, W., Xie, X., Yin, W., Li, H., Liu, M., ... Cheng, Z. (2020). Clinical features of patients infected with 2019 novel coronavirus in Wuhan, China. *The Lancet*, 395(10223), 497–506. [https://doi.org/10.1016/S0140-6736\(20\)30183-5](https://doi.org/10.1016/S0140-6736(20)30183-5)
- Kaiser, J. (2005). Science resources. Chemists want NIH to curtail database. *Science*, 308(5723), 774. <https://doi.org/10.1126/science.308.5723.774a>
- Kamiya, Y., Takaku, H., Yamada, R., Akase, C., Abe, Y., Sekiguchi, Y., Murayama, N., Shimizu, M., Kitajima, M., Shono, F., Funatsu, K., & Yamazaki, H. (2020). Determination and prediction of permeability across intestinal epithelial cell monolayer of a diverse range of industrial chemicals/drugs for estimation of oral absorption as a putative marker of hepatotoxicity. *Toxicology Reports*, 7, 149–154. <https://doi.org/10.1016/j.toxrep.2020.01.004>
- Kang, S., Yang, M., Hong, Z., Zhang, L., Huang, Z., Chen, X., He, S., Zhou, Z., Zhou, Z., Chen, Q., Yan, Y., Zhang, C., Shan, H., & Chen, S. (2020). Crystal structure of SARS-CoV-2 nucleocapsid protein RNA binding domain reveals potential unique drug targeting sites. *Acta Pharmaceutica Sinica B*, 10(7), 1228–1238. <https://doi.org/10.1016/j.apbsb.2020.04.009>
- Karwath, A., & De Raedt, L. (2006). SMIREP: Predicting chemical activity from SMILES. *Journal of Chemical Information and Modeling*, 46(6), 2432–2444. <https://doi.org/10.1021/ci060159g>
- Karypidou, K., Ribone, S. R., Quevedo, M. A., Persoons, L., Pannecouque, C., Helsen, C., Claessens, F., & Dehaen, W. (2018). Synthesis, biological evaluation and molecular modeling of a novel series of fused 1,2,3-triazoles as potential anti-coronavirus agents. *Bioorganic & Medicinal Chemistry Letters*, 28(21), 3472–3476. <https://doi.org/10.1016/j.bmcl.2018.09.019>
- Kauffmann, K., Gremm, L., Brendt, J., Schiwiy, A., Bluhm, K., Hollert, H., & Büchs, J. (2020). Alternative type of Ames test allows for dynamic mutagenicity detection by online monitoring of respiration activity. *Science of the Total Environment*, 726, 137862. <https://doi.org/10.1016/j.scitotenv.2020.137862>
- Khan, R. J., Jha, R. K., Amera, G. M., Jain, M., Singh, E., Pathak, A., Singh, R. P., Muthukumar, J., & Singh, A. K. (2020). Targeting SARS-CoV-2: A systematic drug repurposing approach to identify promising inhibitors against 3C-like proteinase and 2'-O-ribose methyltransferase. *Journal of Biomolecular Structure and Dynamics*, 1–14. <https://doi.org/10.1080/07391102.2020.1753577>
- Komatsu, T. S., Okimoto, N., Koyama, Y. M., Hirano, Y., Morimoto, G., Ohno, Y., & Tajiri, M. (2020). Drug binding dynamics of the dimeric SARS-CoV-2 main protease, determined by molecular dynamics simulation. *Scientific Reports*, 10(1), 1–11. <https://doi.org/10.1038/s41598-020-74099-5>
- Kortagere, S., Ekins, S., & Welsh, W. J. (2008). Halogenated ligands and their interactions with amino acids: Implications for structure-activity and structure-toxicity relationships. *Journal of Molecular Graphics & Modelling*, 27(2), 170–177. <https://doi.org/10.1016/j.jmkgm.2008.04.001>
- Laskowski, R. A., MacArthur, M. W., & Thornton, J. M. (2006). PROCHECK: Validation of protein-structure coordinates.
- Leite, D. I., Fontes, F. d. V., Bastos, M. M., Hoelz, L. V. B., Bianco, M. d. C. A. D., de Oliveira, A. P., da Silva, P. B., da Silva, C. F., Batista, D. d. G. J., da Gama, A. N. S., Peres, R. B., Villar, J. D. F., Soeiro, M. d. N. C., & Boechat, N. (2018). New 1,2,3-triazole-based analogues of benzimidazole for use against *Trypanosoma cruzi* infection: *In vitro* and *in vivo* evaluations. *Chemical Biology & Drug Design*, 92(3), 1670–1682. <https://doi.org/10.1111/cbdd.13333>
- Li, D., Chen, L., Li, Y., Tian, S., Sun, H., & Hou, T. (2014). ADMET evaluation in drug discovery. 13. Development of *in silico* prediction models for P-glycoprotein substrates. *Molecular Pharmaceutics*, 11(3), 716–726. <https://doi.org/10.1021/mp400450m>
- Li, Y., Meng, Q., Yang, M., Liu, D., Hou, X., Tang, L., Wang, X., Lyu, Y., Chen, X., Liu, K., Yu, A., Zuo, Z., & Bi, H. (2019). Current trends in drug metabolism and pharmacokinetics. *Acta Pharmaceutica Sinica B*, 9(6), 1113–1144. <https://doi.org/10.1016/j.apbsb.2019.10.001>
- Lipinski, C. A. (2004). Lead- and drug-like compounds: The rule-of-five revolution. *Drug Discovery Today. Technologies*, 1(4), 337–341. <https://doi.org/10.1016/j.ddtec.2004.11.007>
- Liu, S., Xiao, G., Chen, Y., He, Y., Niu, J., Escalante, C. R., Xiong, H., Farmer, J., Debnath, A. K., Tien, P., & Jiang, S. (2004). Interaction between heptad repeat 1 and 2 regions in spike protein of SARS-associated coronavirus: Implications for virus fusogenic mechanism and identification of fusion inhibitors. *The Lancet*, 363(9413), 938–947. [https://doi.org/10.1016/S0140-6736\(04\)15788-7](https://doi.org/10.1016/S0140-6736(04)15788-7)
- López-Camacho, E., Godoy, M. J. G., García-Nieto, J., Nebro, A. J., & Aldana-Montes, J. F. (2015). Solving molecular flexible docking problems with metaheuristics: A comparative study. *Applied Soft Computing*, 28, 379–393. <https://doi.org/10.1016/j.asoc.2014.10.049>
- López-González, R., Bautista-Renedo, J., Martínez-Otero, D., Reyes, H., González-Rivas, N., & Cuevas-Yañez, E. (2016). 1, 4-and 1, 5-di (*N*-phthalimidomethyl)-1, 2, 3-triazoles: Crystal structures and density functional theory studies of the alkyne and azide precursors. *Journal of Chemical Research*, 40(5), 308–313. <https://doi.org/10.3184/174751916X14608096414015>
- Macrae, C. F., Bruno, I. J., Chisholm, J. A., Edgington, P. R., McCabe, P., Pidcock, E., Rodriguez-Monge, L., Taylor, R., van de Streek, J., & Wood,

- P. A. (2008). Mercury CSD 2.0—new features for the visualization and investigation of crystal structures. *Journal of Applied Crystallography*, 41(2), 466–470. <https://doi.org/10.1107/S0021889807067908>
- Mandić, L., Benčić, P., Mlinarić-Majerski, K., Liekens, S., Snoeck, R., Andrei, G., Kralj, M., & Basarić, N. (2020). Substituted adamantylphthalimides: Synthesis, antiviral and antiproliferative activity. *Archiv Der Pharmazie*, 353(6), 2000024. <https://doi.org/10.1002/ardp.202000024>
- Mehra, M. R., Desai, S. S., Ruschitzka, F., & Patel, A. N. (2020). Hydroxychloroquine or chloroquine with or without a macrolide for treatment of COVID-19: A multinational registry analysis. *The Lancet*, 1–10. [https://doi.org/10.1016/S0140-6736\(20\)31180-6](https://doi.org/10.1016/S0140-6736(20)31180-6)
- Meo, S. A., Al-Khlaiwi, T., Usmani, A. M., Meo, A. S., Klonoff, D. C., & Hoang, T. D. (2020). Biological and epidemiological trends in the prevalence and mortality due to outbreaks of novel coronavirus COVID-19. *Journal of King Saud University-Science*, 32(4), 2495–2499. <https://doi.org/10.1016/j.jksus.2020.04.004>
- Miao, R., Xia, L.-Y., Chen, H.-H., Huang, H.-H., & Liang, Y. (2019). Improved classification of blood-brain-barrier drugs using deep learning. *Scientific Reports*, 9(1), 8802. <https://doi.org/10.1038/s41598-019-44773-4>
- Myatt, G. J., Ahlberg, E., Akahori, Y., Allen, D., Amberg, A., Anger, L. T., Aptula, A., Auerbach, S., Beilke, L., Bellion, P., Benigni, R., Bercu, J., Booth, E. D., Bower, D., Brigo, A., Burden, N., Cammerer, Z., Cronin, M. T. D., Cross, K. P., ... Hasselgren, C. (2018). In silico toxicology protocols. *Regulatory Toxicology and Pharmacology*, 96, 1–17. <https://doi.org/10.1016/j.yrtph.2018.04.014>
- Ouyang, T., Liu, X., Ouyang, H., & Ren, L. (2018). Recent trends in click chemistry as a promising technology for virus-related research. *Virus Research*, 256, 21–28. <https://doi.org/10.1016/j.virusres.2018.08.003>
- Papadopoulou, M. V., Bloomer, W. D., Rosenzweig, H. S., Kaiser, M., Chatelain, E., & Ioset, J. R. (2013). Novel 3-nitro-1H-1,2,4-triazole-based piperazines and 2-amino-1,3-benzothiazoles as antichagasic agents. *Bioorganic & Medicinal Chemistry*, 21(21), 6600–6607. <https://doi.org/10.1016/j.bmc.2013.08.022>
- Phatak, P. S., Bakale, R. D., Dhumal, S. T., Dahiwade, L. K., Choudhari, P. B., Siva Krishna, V., Sriram, D., & Haval, K. P. (2019). Synthesis, anti-tubercular evaluation and molecular docking studies of phthalimide bearing 1, 2, 3-triazoles. *Synthetic Communications*, 49(16), 2017–2028. <https://doi.org/10.1080/00397911.2019.1614630>
- Piñana, J., Montoro, J., Aznar, C., Lorenzo, I., Gómez, M. D., Guerreiro, M., Carretero, C., González-Barberá, E. M., Balaguer-Roselló, A., Sanz, R., Salavert, M., Navarro, D., Sanz, M. A., Sanz, G., & Sanz, J. (2020). The clinical benefit of instituting a prospective clinical community-acquired respiratory virus surveillance program in allogeneic hematopoietic stem cell transplantation. *Journal of Infection*, 80(3), 333–341. <https://doi.org/10.1016/j.jinf.2019.12.022>
- Pires, D. E., Blundell, T. L., & Ascher, D. B. (2015). pkCSM: Predicting small-molecule pharmacokinetic and toxicity properties using graph-based signatures. *Journal of Medicinal Chemistry*, 58(9), 4066–4072. <https://doi.org/10.1021/acs.jmedchem.5b00104>
- Razzaghi-Asl, N., Ebadi, A., Shahabipour, S., & Gholamin, D. (2020). Identification of a potential SARS-CoV2 inhibitor via molecular dynamics simulations and amino acid decomposition analysis. *Journal of Biomolecular Structure and Dynamics*, 1–16. <https://doi.org/10.1080/07391102.2020.1797536>
- Ronnebaum, J. M., & Luzzio, F. A. (2016). Synthesis of 1, 2, 3-triazole 'click' analogues of thalidomide. *Tetrahedron*, 72(40), 6136–6141. <https://doi.org/10.1016/j.tet.2016.07.019>
- Sadat-Ebrahimi, S. E., Rahmani, A., Mohammadi-Khanapostani, M., Jafari, N., Mojtavavi, S., Ali Faramarzi, M., Emadi, M., Yahya-Meymandi, A., Larijani, B., Biglar, M., & Mahdavi, M. (2020). New phthalimide-benzamide-1, 2, 3-triazole hybrids; design, synthesis, α -glucosidase inhibition assay, and docking study. *Medicinal Chemistry Research*, 29(5), 868–869. <https://doi.org/10.1007/s00044-020-02522-7>
- Sanchis-Gomar, F., Lavie, C. J., Perez-Quilis, C., Henry, B. M., & Lippi, G. (2020). Angiotensin-Converting Enzyme 2 and antihypertensives (angiotensin receptor blockers and angiotensin-converting enzyme inhibitors) in Coronavirus Disease 2019. *Mayo Clinic Proceedings*, 95(6), 1222–1230. <https://doi.org/10.1016/j.mayocp.2020.03.026>
- Singh, S., El-Sakkary, N., Skinner, D. E., Sharma, P. P., Ottilie, S., Antonova-Koch, Y., Kumar, P., Winzeler, E., Poonam, Caffrey, C., & Rathi, B. (2020). Synthesis and bioactivity of phthalimide analogs as potential drugs to treat schistosomiasis, a neglected disease of poverty. *Pharmaceuticals*, 13(2), 25. <https://doi.org/10.3390/ph13020025>
- Stewart, J. J. (1989). Optimization of parameters for semiempirical methods II. *Journal of Computational Chemistry*, 10(2), 221–264. <https://doi.org/10.1002/jcc.540100209>
- Sun, L., Huang, T., Dick, A., Meuser, M. E., Zalloum, W. A., Chen, C. H., Ding, X., Gao, P., Cocklin, S., Lee, K., Zhan, P., & Liu, X. (2020). Design, synthesis and structure-activity relationships of 4-phenyl-1H-1,2,3-triazole phenylalanine derivatives as novel HIV-1 capsid inhibitors with promising antiviral activities. *European Journal of Medicinal Chemistry*, 190, 112085. <https://doi.org/10.1016/j.ejmech.2020.112085>
- Surjit, M., Liu, B., Chow, V. T., & Lal, S. K. (2006). The nucleocapsid protein of severe acute respiratory syndrome-coronavirus inhibits the activity of cyclin-cyclin-dependent kinase complex and blocks S phase progression in mammalian cells. *Journal of Biological Chemistry*, 281(16), 10669–10681. <https://doi.org/10.1074/jbc.M509233200>
- Tehrani, M. B., Emani, P., Rezaei, Z., Khoshneviszadeh, M., Ebrahimi, M., Edraki, N., Mahdavi, M., Larijani, B., Ranjbar, S., Foroumadi, A., & Khoshneviszadeh, M. (2019). Phthalimide-1, 2, 3-triazole hybrid compounds as tyrosinase inhibitors; synthesis, biological evaluation and molecular docking analysis. *Journal of Molecular Structure*, 1176, 86–93. <https://doi.org/10.1016/j.molstruc.2018.08.033>
- Tetko, I. V., Varbanov, H. P., Galanski, M., Talmaciu, M., Platts, J. A., Ravera, M., & Gabano, E. (2016). Prediction of logP for Pt(II) and Pt(IV) complexes: Comparison of statistical and quantum-chemistry based approaches. *Journal of Inorganic Biochemistry*, 156, 1–13. <https://doi.org/10.1016/j.jinorgbio.2015.12.006>
- Thanh, N. D., Hai, D. S., Ngoc Bich, V. T., Thu Hien, P. T., Ky Duyen, N. T., Mai, N. T., Dung, T. T., Toan, V. N., Kim Van, H. T., Dang, L. H., Toan, D. N., & Thanh Van, T. T. (2019). Efficient click chemistry towards novel 1H-1,2,3-triazole-tethered 4H-chromene-d-glucose conjugates: Design, synthesis and evaluation of in vitro antibacterial, MRSA and antifungal activities. *European Journal of Medicinal Chemistry*, 167, 454–471. <https://doi.org/10.1016/j.ejmech.2019.01.060>
- Tkatchenko, A., & Scheffler, M. (2009). Accurate molecular van der Waals interactions from ground-state electron density and free-atom reference data. *Physical Review Letters*, 102(7), 073005. <https://doi.org/10.1103/PhysRevLett.102.073005>
- Utomo, R. Y., & Meiyanto, E. (2020). Revealing the potency of citrus and galangal constituents to halt SARS-CoV-2 infection. *Preprint*, 1, 1–8. <https://doi.org/10.20944/preprints202003.0214.v1>
- Walls, A. C., Park, Y. J., Tortorici, M. A., Wall, A., McGuire, A. T., & Veesler, D. (2020). Structure, function, and antigenicity of the SARS-CoV-2 spike glycoprotein. *Cell*, 183(6), 1735. <https://doi.org/10.1016/j.cell.2020.02.058>
- Wrapp, D., Wang, N., Corbett, K. S., Goldsmith, J. A., Hsieh, C. L., Abiona, O., Graham, B. S., & McLellan, J. S. (2020). Cryo-EM structure of the 2019-nCoV spike in the prefusion conformation. *Science*, 367(6483), 1260–1263. <https://doi.org/10.1126/science.abb2507>
- Xu, L., Jiang, W., Jia, H., Zheng, L., Xing, J., Liu, A., & Du, G. (2020). Discovery of multitarget-directed ligands against influenza A virus from compound yizhihao through a predictive system for compound-protein interactions. *Frontiers in Cellular and Infection Microbiology*, 10, 16. <https://doi.org/10.3389/fcimb.2020.00016>
- Yadav, R., Imran, M., Dhamija, P., Suchal, K., & Handu, S. (2020). Virtual screening and dynamics of potential inhibitors targeting RNA binding domain of nucleocapsid phosphoprotein from SARS-CoV-2. *Journal of Biomolecular Structure and Dynamics*, 1–16. <https://doi.org/10.1080/07391102.2020.1778536>
- Yang, R., Liu, H., Bai, C., Wang, Y., Zhang, X., Guo, R., Wu, S., Wang, J., Leung, E., Chang, H., Li, P., Liu, T., & Wang, Y. (2020). Chemical composition and pharmacological mechanism of Qingfei Paidu Decoction and Ma Xing Shi Gan Decoction against Coronavirus Disease 2019 (COVID-19): In silico and experimental study. *Pharmacological Research*, 157, 104820. <https://doi.org/10.1016/j.phrs.2020.104820>
- Zeng, Y., Ye, L., Zhu, S., Zheng, H., Zhao, P., Cai, W., Su, L., She, Y., & Wu, Z. (2008). The nucleocapsid protein of SARS-associated coronavirus inhibits B23

- phosphorylation. *Biochemical and Biophysical Research Communications*, 369(2), 287–291. <https://doi.org/10.1016/j.bbrc.2008.01.096>
- Zhang, W., Zhao, Y., Zhang, F., Wang, Q., Li, T., Liu, Z., Wang, J., Qin, Y., Zhang, X., Yan, X., Zhang, X., Yan, Z., Zeng, X., & Zhang, S. (2020). The use of anti-inflammatory drugs in the treatment of people with severe coronavirus disease 2019 (COVID-19): The experience of clinical immunologists from China. *Clinical Immunology (Orlando, FL)*, 214, 108393. <https://doi.org/10.1016/j.clim.2020.108393>
- Zhou, B., Liu, J., Wang, Q., Liu, X., Li, X., Li, P., Ma, Q., & Cao, C. (2008). The nucleocapsid protein of severe acute respiratory syndrome coronavirus inhibits cell cytokinesis and proliferation by interacting with translation elongation factor 1alpha. *Journal of Virology*, 82(14), 6962–6971. <https://doi.org/10.1128/JVI.00133-08>
- Zhou, R., Zeng, R., von Brunn, A., & Le, J. (2020). Structural characterization of the C-terminal domain of SARS-CoV-2 nucleocapsid protein. *Molecular Biomedicine*, 1(1), 3–11. <https://doi.org/10.1186/s43556-020-00001-4>